

Flavor conversion of cosmic neutrinos from hidden jets

Soebur Razzaque^{a,b*} and A. Yu. Smirnov^{c,d†}

^a*Space Science Division, U.S. Naval Research Laboratory,
4555 Overlook Ave. SW, Washington, DC 20375, USA*

^b*National Research Council Research Associate*

^c*The Abdus Salam International Centre for Theoretical Physics,
Strada Costiera 11, I-34014 Trieste, Italy*

^d*Institute for Nuclear Research, Russian Academy of Sciences, Moscow, Russia*

ABSTRACT: High energy cosmic neutrino fluxes can be produced inside relativistic jets under the envelopes of collapsing stars. In the energy range $E \sim (0.3 - 10^5)$ GeV, flavor conversion of these neutrinos is modified by various matter effects inside the star and the Earth. We present a comprehensive (both analytic and numerical) description of the flavor conversion of these neutrinos which includes: (i) oscillations inside jets, (ii) flavor-to-mass state transitions in an envelope, (iii) loss of coherence on the way to observer, and (iv) oscillations of the mass states inside the Earth. We show that conversion has several new features which are not realized in other objects, in particular interference effects (“L- and H-wiggles”) induced by the adiabaticity violation. The $\nu - \nu$ scattering inside jet and inelastic neutrino interactions in the envelope may produce some additional features at $E \gtrsim 10^4$ GeV. We study dependence of the probabilities and flavor ratios in the matter-affected region on angles θ_{13} and θ_{23} , on the CP-phase δ , as well as on the initial flavor content and density profile of the star. We show that measurements of the energy dependence of the flavor ratios will, in principle, allow to determine independently the neutrino and astrophysical parameters.

KEYWORDS: Neutrino Physics, Electromagnetic Processes and Properties.

*email: srazzaque@ssd5.nrl.navy.mil

†email: smirnov@ictp.it

Contents

1. Introduction	2
2. Neutrinos from jets: production, physical conditions, fluxes	4
2.1 Properties of relativistic jets	4
2.2 Proton acceleration	6
2.3 Neutrino fluxes from meson decays	6
2.4 Stellar envelope: density profile	9
2.5 Neutrino fluxes and densities	10
2.6 Coherence and averaging	10
2.7 Effect of inelastic interactions	11
3. Conversion inside the star: general consideration	12
3.1 Propagation basis	12
3.2 General expressions for probabilities	13
3.3 Matter affected range	15
3.4 Asymptotic values of probabilities	17
3.5 Adiabatic conversion	17
3.6 Adiabaticity breaking	20
3.7 H-wiggles	21
3.8 L-wiggles	24
3.9 Dependence on the density profile	27
4. Properties of conversion probabilities	28
4.1 Probabilities of $\nu_e \rightarrow \nu_\beta$ transitions	28
4.2 Probabilities of $\nu_\mu \rightarrow \nu_\beta$ and $\nu_\tau \rightarrow \nu_\beta$ transitions	31
4.3 Probabilities in antineutrino channels	32
4.4 Probabilities for the inverted mass hierarchy	33
4.5 Effects of oscillations inside jets	35
4.6 CP-violation effects	38
5. Fluxes at the Earth	41
5.1 Flavor ratios	41
5.2 Properties of the flavor ratios	42
6. Discussion and conclusion	47
A. Meson and lepton energy losses	51
B. Comparison of the conversion formulas in Ref. [16] and in this paper	52

1. Introduction

It is difficult to overestimate importance of future detection of high energy cosmic neutrinos which will open new window to the Universe (for reviews see e.g. [1]). This detection will bring unique information on astrophysical sources of the neutrinos, as well as on neutrinos themselves: their propagation, interactions and flavor conversion. A number of different high-energy, $\gtrsim 1$ GeV, neutrino sources have been proposed in literature, which includes active galactic nuclei (AGNs) [2], gamma ray bursts (GRBs) [3], core collapse supernovae (SNe) [4], supernova remnants [5], etc. Properties of neutrino fluxes, energy range, shape of the energy spectra and flavor content depend on physical conditions in the sources, as well as on effects of propagation between the source and the Earth. In particular, the flavor content of fluxes is modified by the vacuum oscillations between the production region and the Earth-based detectors. For known neutrino mass squared differences the oscillations are averaged due to large distances (baselines), and the oscillation effects are described by the averaged vacuum oscillation probabilities which do not depend on neutrino energy.

The sources listed above are detected by their electromagnetic (EM) radiation with space- and ground-based detectors. No astrophysical source has been detected so far by its high energy neutrino signal. Apart from the sources visible in EM radiation, it is expected that there are various hidden sources of neutrinos: the sources in which the EM radiation produced in the inner part of the object is absorbed in the surrounding dense material and only neutrinos can pass through and be detected at the Earth. One such optically thick source is a core collapse SN with mildly relativistic jets emitted by a central engine, a black hole or a highly magnetized neutron star. These jets form promptly after the collapse [6] and may not break the envelope unlike highly-relativistic GRB jets. Therefore they may not lead to emission of high energy non-thermal EM radiation. Observation of late time radio afterglow and explosion geometry provide evidences of a plausible hidden jet in some SNe [7]. These hidden jets, however, can be the sources of high-energy neutrino fluxes generated by interactions of the shock accelerated protons with surrounding matter and radiation [6, 8, 9].

The number of hidden sources can be much larger than the number of observable ones, limited only by the ratio of type Ib/c and type II SNe to GRB rates. The combined SN rate from roughly 4000 galaxies within 20 Mpc is larger than one per year and the SN rate in nearby starburst galaxies such as M82 and NGC253 is much higher than in the Milky way [6, 10]. Recent γ -ray observation of M82 and NGC253 with the Fermi Large Area Space Telescope also supports an increased SN activity [11]. The prospect of high-energy neutrino detection from SNe in these galaxies by neutrino detectors such as IceCube[12] ANTARES [13] and KM3NeT [14] is rather high, if a significant fraction of the SNe are endowed with mildly-relativistic jets. Optical follow-up triggered by neutrino events in

IceCube along the direction of the neutrino trajectories will further enhance detection prospect by identifying the SN and extrapolating its light curve back to the explosion time [15].

Neutrinos produced in the hidden jets cross an envelope and in [16] it was shown that in general matter effects on neutrino oscillations are not small. In particular, the minimal width condition (the lower bound on the column density of electrons on the way of neutrinos which is required for strong matter effect) [17] can be satisfied. It was shown that the matter effects inside a star can substantially modify the average vacuum oscillation probabilities in the range from 10^2 GeV (the IceCube threshold) up to 10^5 GeV. Neutrino fluxes at the surface of the Earth have been computed. As an observable in the forthcoming experiments, the ratio of shower events (induced mainly by the electron and tau neutrinos) and the muon track events (produced mainly by interactions of muon neutrinos and antineutrinos) has been proposed [16]. The ratio as a function of energy depends on values of the mixing angles θ_{13} , θ_{23} , the CP-violation phase δ as well as on density profiles of the stellar envelope. It was concluded, in particular, that with about 10^3 events one can explore the neutrino properties such as the type of mass hierarchy and CP violating phase, provided that the mixing angles will be measured at future reactor and accelerator experiments with high accuracy. Also certain information about properties of the source can be extracted. The rate of detection of individual source from nearby galaxies is one in 5–10 years. If the neutrino telescopes are able to detect the diffuse flux of neutrinos from all the sources, still one can see some deviation of the flavor ratio from that produced by the vacuum oscillations. Inversely, observation of such a deviation in certain energy range can be explained by matter induced transformations and large population of the hidden sources. With high statistics this feature in the energy spectrum can be extracted from large background of atmospheric neutrinos.

In this paper we have reconsidered the flavor conversion of neutrinos from hidden jets. Our results differ from those in Ref. [16]. The difference originates from treatment of averaging and the coherence loss. Neutrinos produced by pions, muons and kaons in the strong magnetic field have very short wave packets and lose coherence due to separation of the wave packets [18]. So, neutrinos arrive at the surface of the Earth as incoherent fluxes of the mass eigenstates and coherence is not restored in detector. Therefore one should compute probabilities of the flavor-to-mass transitions ($\nu_\alpha \rightarrow \nu_i$) inside the star. In contrast, in Ref. [16] the flavor-to-flavor transitions have been computed from the production point to the surface of the star and then the oscillations on the way from the surface of the star to the earth have been averaged. This leads to different results of numerical computations. In particular, fast oscillatory behavior of probabilities with energy appears according to [16]. We have included in consideration also additional effects not considered in [16], such as energy-dependent particle to antiparticle ratio and flavor ratio in the initial neutrino fluxes, oscillations in jets, inelastic interactions of neutrinos and neutrino-neutrino scattering. Detailed and comprehensive study of the conversion inside the star and on the way between the star and the Earth is performed. We show that the main effect is due to the adiabatic and partially adiabatic conversion (the MSW-effect) [19] inside an envelope. Both numerical and analytical results for probabilities, neutrino fluxes and flavor ratios at

the Earth are presented. Computation of number of events in specific detectors is beyond the scope of this paper and will be given elsewhere.

The paper is organized as follows. In Sec. 2 we describe the model of hidden source, summarize physical conditions at the neutrino production site, and present properties of the generated neutrino fluxes. We describe neutrino conversion inside the star in Sec. 3 that includes the adiabatic conversion at low energies, adiabaticity violation at energies above the 1-3 resonance, interference effects in the range of adiabaticity violation which lead to H- and L- wiggles. We describe properties of the conversion probabilities in specific channels, their dependence on neutrino parameters and characteristic of density profiles in Sec. 4. In Sec. 5 we present neutrino fluxes and flavor ratios at the surface of the Earth. We consider their dependence on neutrino parameters, original flavor content as well as on the density profile of the stellar envelope. Conclusions are presented in Sec. 6. Some details of neutrino flux calculation, explanation of the difference of results of [16] and this paper, and details of estimations of the Earth matter effects are presented in Appendices A, B and C correspondingly.

2. Neutrinos from jets: production, physical conditions, fluxes

Here we discuss generic properties of source, conditions of neutrino production and characteristics of neutrino fluxes.

2.1 Properties of relativistic jets

Hidden neutrino sources are associated to the core collapses of stars with masses $M_\star \lesssim 28M_\odot$. Models of these sources are based on extrapolation of the observed properties of GRB and models of observed jets. Recall that stars with mass $M_\star \gtrsim 28M_\odot$ and a fast-rotating core are widely believed to be the progenitors of the long-duration GRBs [20]. Evidences of highly relativistic jets, with bulk Lorentz factor $\Gamma_b \sim 10^2 - 10^3$, have been found in recent GRB data [21].

A much larger number of core-collapses with masses of progenitors $M_\star \lesssim 28M_\odot$ is believed to produce mildly relativistic, $\Gamma_b \sim 10^{0.5} - 10^1$, *slow* jets which do not break through the stellar envelope unlike the GRB jets [22]. The general picture is that materials from the central engine (a black hole or a highly magnetized neutron star created from the core-collapse) are emitted in lumps or shells with mildly relativistic speeds along the rotation axis of the star, thus forming a slow jet. Some initial shell or shells push out stellar material (with sub-relativistic or mildly-relativistic speed), thus make a cavity. Subsequent shells, with relativistic speed in the cavity, collide with each other due to variable outflow of accreting materials similar to the GRB internal shocks which take place well outside the stellar envelope (for reviews see e.g. [23]). Each of these binary collisions produce shock waves (forward and reverse) in the colliding shells. The shell(s), initially ejected, can also produce a shock in the envelope (forward shock), and a reflected shock (reverse shock) in the shell(s). The shock in the envelope dissipates very quickly because of a higher density, but could also accelerate particles there.

The subsequent binary collisions between the shells take place mainly at the edge of the jet or at the inner border of the envelope. The shock waves that are generated in the leading and trailing shells, in a binary collision, are mildly relativistic, with the Lorentz factor ~ 1 in the frame of the shells which, in turn, are moving at the Lorentz factor ~ 3 in the observer frame [6]. As these shock waves traverse the shells, magnetic field is generated from turbulence in the upstream and downstream regions of the shock front. The magnetic fields in these two regions are similar.

The shocks in the hidden or burried jets are optically thick to γ -rays as they are produced under the stellar envelope. High energy neutrino fluxes, however, are formed inside the slow jet due to interactions of shock-accelerated protons with matter, (pp -collisions) and EM radiation ($p\gamma$ - collisions) of jets [6, 8].

Following Refs. [6, 9] we adopt a slow jet model with the following characteristics:

- the total kinetic energy of the jet released over its duration is $E_j \sim 10^{51.5} E_{51.5}$ ergs which is much smaller than the typical GRB jet energy;
- the jet duration is $t_j \sim 10 t_{j,1}$ s, which is the typical duration of the central engine's activity observed in GRBs;
- the half angle of the jet, $\theta_j \sim 1/\Gamma_b$, is rather large and implies an isotropic-equivalent total jet energy $E_{j,\text{iso}} \approx 2\Gamma_b^2 E_j$;
- with a variability time scale $t_v \sim 0.1 t_{v,-1}$ s and $\Gamma_b \sim 10^{0.5} \Gamma_{b,0.5}$, the internal shocks (collision between two shells) take place at a radius $r_j \approx 2\Gamma_b^2 c t_v \sim 6.3 \cdot 10^{10} \Gamma_{b,0.5}^2 t_{v,-1}$ cm;
- the width of the shocked shells is $\Delta r_j \approx r_j / \Gamma_b^2 \sim 6.3 \cdot 10^9 t_{v,-1}$ cm and there can be $\approx t_j / 2t_v \sim 50$ consecutive collisions between shells which form shocks in the shells during the jet lifetime.

This picture is somewhat idealized since GRB data show more complex time structure than emission from identical shocked shells. Nevertheless, it captures the basic scenario of internal shocks.

The pre-shock number density of particles in the jet calculated in the jet comoving frame (we denote the corresponding characteristics by “ r ”) is

$$n'_e \simeq n'_p \approx \frac{E_{j,\text{iso}}}{4\pi r_j^2 \Gamma_b^2 t_j m_p} \sim 3.2 \cdot 10^{20} \text{ cm}^{-3} \frac{E_{51.5}}{\Gamma_{b,0.5}^4 t_{j,1} t_{v,-1}^2}. \quad (2.1)$$

(Here and below $\hbar = c = 1$.) The post-shock number density is $\approx 4n'_p$ and the strength of magnetic field that forms due to turbulence in the shock region is

$$B' \approx \sqrt{32\pi \epsilon_B n'_p m_p} \sim 6.3 \cdot 10^8 \text{ G} \sqrt{\frac{\epsilon_{B,-2} E_{51.5}}{\Gamma_{b,0.5}^4 t_{j,1} t_{v,-1}^2}}, \quad (2.2)$$

where $\epsilon_B \sim 10^{-2} \epsilon_{B,-2}$ is the fraction of shock energy that goes into creating magnetic field. The magnetic field drops down to the surrounding value of few Gauss (which is the

field from the “central engine”, a magnetar or black hole) between successive shocks. The temperature of the thermal photons, created by shocked electrons which carry a fraction $\epsilon_e \sim 10^{-1} \epsilon_{e,-1}$ of the total energy, in the jet equals

$$kT' \approx \left(\frac{15}{\pi^2} \frac{\epsilon_e E_{j,\text{iso}}}{4\pi r_j^2 \Gamma_b^2 t_j} \right)^{1/4} \sim 4.3 \text{ keV} \left(\frac{\epsilon_{e,-1} E_{51.5}}{\Gamma_{b,0.5}^4 t_{j,1} t_{v,-1}^2} \right)^{1/4}. \quad (2.3)$$

2.2 Proton acceleration

We consider a Fermi acceleration mechanism for protons in shocks. An acceleration time scale is proportional to the Larmor time scale and equals

$$t'_{p,\text{acc}} \approx \frac{\varphi}{m_p^2} \frac{B_{\text{cr}}}{B'} E'_p \sim 10^{-9} \text{ s } \varphi_1 \left(\frac{E'_p}{\text{TeV}} \right) \left(\frac{B'}{10^9 \text{ G}} \right)^{-1},$$

where $B_{\text{cr}} = m_p^2/q \approx 1.488 \times 10^{20} \text{ G}$ is the critical magnetic field and $\varphi \sim 10\varphi_1$ is the number of gyro-radii required to increase the particle energy by e -fold. We assume an acceleration spectrum $N(E_p) \propto E_p^{-2}$. Then the differential flux of protons, if they could escape freely from the jet, at a luminosity distance d_L would be

$$\Phi_p(E_p) \approx \frac{E_{j,\text{iso}}}{4\pi d_L^2 E_p^2 t_j \ln(E_{p,\text{max}}/\Gamma_b m_p)}. \quad (2.4)$$

The maximum proton energy is determined by the shortest time scale for energy losses which is the synchrotron cooling time scale

$$t'_{p,\text{syn}} \approx \frac{9}{4} \frac{1}{r_e m_e} \left(\frac{B_{\text{cr}}}{B'} \right)^2 \frac{1}{E'_p} \sim 2 \cdot 10^{-2} \text{ s} \left(\frac{E'_p}{\text{TeV}} \right)^{-1} \left(\frac{B'}{10^9 \text{ G}} \right)^{-2}.$$

In the jet frame this gives

$$E'_{p,\text{max}} \approx \sqrt{\frac{9}{4} \frac{m_p^2}{\varphi r_e m_e} \frac{B_{\text{cr}}}{B'}} \sim 2 \cdot 10^3 \text{ TeV } \varphi_1^{-1/2} \left(\frac{B'}{10^9 \text{ G}} \right)^{-1/2}. \quad (2.5)$$

and consequently, in the observer’s frame $E_{p,\text{max}} = \Gamma_b E'_{p,\text{max}} \sim 6.3 \cdot 10^3 \text{ TeV}$. In turn, this energy determines the maximal energy of the neutrino spectrum.

2.3 Neutrino fluxes from meson decays

The rate of pp - interaction by shock-accelerated protons in the jet is given by

$$\begin{aligned} K_{pp}(E'_p) &\approx n'_p \sigma_{pp}(E'_p) \\ &\sim 3 \cdot 10^5 \text{ s}^{-1} \left[1 + 0.0548 \ln \left(\frac{E'_p}{\text{TeV}} \right) + 0.0073 \ln^2 \left(\frac{E'_p}{\text{TeV}} \right) \right], \end{aligned}$$

where σ_{pp} is the total inelastic cross-section and the parameterization is valid for $E'_p \gtrsim 10 \text{ GeV}$. The scattering rate of $p\gamma$ - interactions with thermal photons in the jet above the

threshold of π -production is given by

$$\begin{aligned}
 K_{p\gamma}(E'_p) &\approx \frac{m_p^2}{2E_p'^2} \int_0^\infty d\varepsilon' \frac{n'_\gamma(\varepsilon)}{\varepsilon^2} \int_{\varepsilon_{\text{th}}}^{2E'_p\varepsilon'/m_p} d\varepsilon_r \varepsilon_r \sigma_{p\gamma}(\varepsilon_r) \\
 &\sim \frac{\sigma_0}{\pi^2} \int_{\varepsilon'_{\text{th}} m_p/2E'_p}^\infty d\varepsilon' \frac{\varepsilon'^2}{\exp[\varepsilon'/kT'] - 1} \sim 10^7 \text{ s}^{-1}.
 \end{aligned}$$

Here $\varepsilon'_r = \varepsilon'(1 - \beta_p \cos \theta)E'_p/m_p$ is the photon energy evaluated in the proton's rest frame for the angle θ between the directions of the proton and target photon. We used for simplicity a constant, $p\gamma$ cross-section $\sigma_{p\gamma}(\varepsilon'_r) \sim \sigma_0 \sim 200\mu\text{b}$, above a threshold photon energy $\varepsilon'_r \approx \varepsilon'_{\text{th}} \approx 0.2 \text{ GeV}$ for pion production in the rest frame of the proton. The threshold energy of protons which produce pions in the $p\gamma$ - interactions equals according to (2.3)

$$E'_{p,\text{th}} \gtrsim \frac{\varepsilon'_{\text{th}} m_p}{kT'} \approx 42 \text{ TeV}.$$

Thus, the pp - scattering rate dominates below $E_{p,\text{th}} \lesssim E'_{p,\text{th}} \Gamma_b \sim 133 \text{ TeV}$, that is the whole energy range of interest.

The fluxes of π - and K - mesons from the pp - or $p\gamma$ - interaction at production can be calculated as

$$\Phi_{\pi(K)}(E_{\pi(K)}) = \int dE_p \Phi_p(E_p) K_{pp/p\gamma}(E'_p) t'_{\text{dyn}} \frac{Y_{\pi(K)}}{E_p}, \quad (2.6)$$

where $Y_{\pi(K)} \equiv E_p (dn_{\pi(K)}/dE_{\pi(K)})$ is the pion (kaon) yield function from the pp - or $p\gamma$ - interactions, and $t'_{\text{dyn}} = r_j/\Gamma_b$ is the dynamic or light crossing time. The quantity $K_{pp/p\gamma}(E'_p) t'_{\text{dyn}}$ is equivalent to the optical depth of the respective interactions and is very large for both the pp - and $p\gamma$ - processes. For roughly constant values of $K_{pp/p\gamma}(E'_p) t'_{\text{dyn}}$ the integral in (2.6) corresponds to the fraction of the proton beam energy carried by π^+ ($f_{\pi^+} \sim 17\%$) and K^+ ($f_{K^+} \sim 2\%$) mesons and follow the primary proton spectrum [24]. Thus the corresponding spectra at production can be estimated as

$$\Phi_{\pi^+(K^+)}^0(E_{\pi(K)}) \sim \frac{f_{\pi^+(K^+)} E_{j,\text{iso}}}{4\pi d_L^2 E_{\pi(K)}^2 t_j \ln(E_{p,\text{max}}/\Gamma_b m_p)}, \quad (2.7)$$

following Eq. (2.4). For the π^- and K^- fluxes the fraction of the proton beam energy carried by the mesons are $f_{\pi^-} \sim 13\%$ and $f_{K^-} \sim 1\%$, respectively. Charm production and semi-leptonic decay contribute to neutrino flux at very high energies [25], which we ignore for the present discussion.

We use the decay constants listed in Ref. [26] to calculate the neutrino fluxes from the direct decay channels $\pi/K \rightarrow \nu_\mu$, the chain decay channels $\pi/K \rightarrow \mu \rightarrow \nu_\mu \nu_e$ and the $K^+ \rightarrow \pi^0 e^+ \nu_e$ decay channels by taking into account their energy losses (see Appendix A). The fluxes are plotted in Fig. 1. Note that very high-energy neutrinos interact inelastically with nucleons in the stellar envelope and are subject to absorption. We discuss this issue in Sec. 2.7.

The ratios of the ν_e to ν_μ and $\bar{\nu}_e$ to $\bar{\nu}_\mu$ fluxes can be fitted reasonably well as

$$\begin{aligned}\epsilon(E) &\equiv \frac{\Phi_{\nu_e}^0}{\Phi_{\nu_\mu}^0} \approx \frac{13.9}{(E_\nu/\text{GeV})^{1.65}} [\Theta(E_\nu - 10 \text{ GeV}) + \Theta(45 \text{ GeV} - E_\nu)] \\ &\quad + 0.0265 [\Theta(E_\nu - 45 \text{ GeV}) + \Theta(10^4 \text{ GeV} - E_\nu)] ; \\ \bar{\epsilon}(E) &\equiv \frac{\Phi_{\bar{\nu}_e}^0}{\Phi_{\bar{\nu}_\mu}^0} \approx \frac{7.85}{(E_\nu/\text{GeV})^{1.5}} [\Theta(E_\nu - 10 \text{ GeV}) + \Theta(45 \text{ GeV} - E_\nu)] \\ &\quad + 0.0265 [\Theta(E_\nu - 45 \text{ GeV}) + \Theta(10^4 \text{ GeV} - E_\nu)] ,\end{aligned}\quad (2.8)$$

where $\Theta(x \geq 0) = 1$ and $\Theta(x < 0) = 0$. The ratios decrease from the initial value because of a decreasing contribution to the ν_e -flux from the chain $\pi - \mu$ decays, and becomes constant at higher energy because of an approximately constant ratio between the ν_e -flux from $K^+ \rightarrow \pi^0 e^+ \nu_e$ and ν_μ -flux from $K^+ \rightarrow \mu^+ \nu_\mu$ channels.

The flux of muon neutrinos in the production region (the $r_j \sim 6.3 \cdot 10^{10}$ cm) and for a jetted source at 10 Mpc can be parameterized, with a piece-wise power-law function, as

$$\frac{E^2 \Phi_{\nu_\mu}}{\text{GeV cm}^{-2} \text{ s}^{-1}} = \begin{cases} 1.64 ; 1 < E/\text{GeV} < 6, \\ 1.64 (E/6 \text{ GeV})^{-0.55} ; 6 \leq E/\text{GeV} \leq 600, \\ 0.13 (E/600 \text{ GeV})^{-1} ; 600 < E/\text{GeV} \leq 3 \times 10^4 . \end{cases}$$

This fit reproduces exactly the ν_μ flux plotted in Fig. 1 below and above 6 GeV and 600 GeV, respectively, and deviates by at most 30% from the numerical flux within 6-600 GeV. We use the numerical flux values for all our calculations.

The ratio of neutrino and antineutrino fluxes can be as large as $\Phi_\nu/\Phi_{\bar{\nu}} \sim 1.5$ because of the preferential production of π^+ and K^+ over π^- and K^- . Indeed, in the pp -collisions the leading pion (which gives main contribution to neutrino flux) is positive. In $p\gamma$ - collisions there is a leading π^+ , although the secondary neutron with roughly 85% of the initial proton's energy will interact further and produce a π^- .

This effect is present in the atmospheric neutrino fluxes, however the ratio of neutrino and antineutrino fluxes and details of the energy dependence is different in our situation. The original flavor content is thus,

$$\epsilon(E) : 1 : 0 \quad \text{and} \quad \bar{\epsilon}(E) : 1 : 0 ,\quad (2.9)$$

where $\epsilon(E)$ and $\bar{\epsilon}(E)$ decrease from 0.5 at low energies down to 10^{-2} at high energies.

The charged π , K mesons and muons can also be accelerated in the shocks [27] similarly to the protons, with a maximum energy $E_{\pi;K,\text{max}} = (m_{\pi;K}/m_p)^2 E_{p,\text{max}}$ following Eq. (2.5). Although a detail study is lacking, it might be possible that π , K and μ decay without suffering severe energy losses. In such a scenario, the flux ratio $1 : 2 : 0$ will be maintained to high energies. In reality one can expect some intermediate situation between this flavor content and the one in Eq. (2.9) without acceleration of mesons. In what follows we will present computations for both extreme flavor contents.

The parent mesons and muons are isotropically distributed in the shocked region because of their small Larmor radius in the large magnetic field. Therefore the neutrinos are also isotropically produced in the comoving frame. However in the observer frame they are

emitted mostly along the jet direction similar to the relativistic beaming effect for photons. Then neutrinos, produced in the low-density jet, propagate through the stellar envelope.

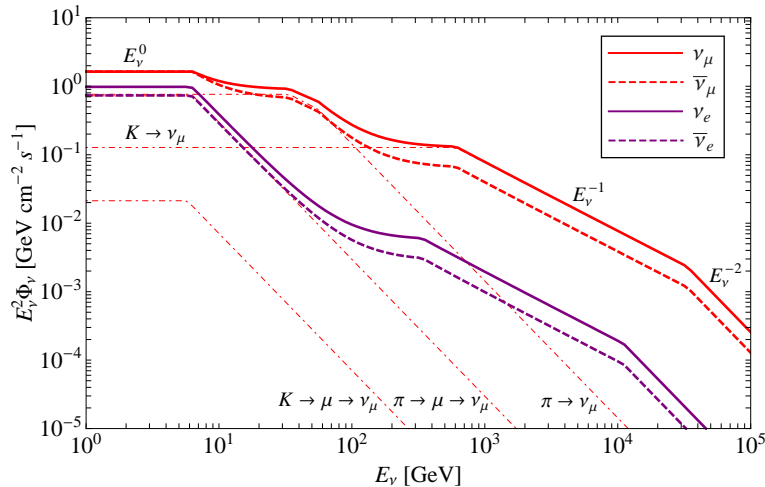


Figure 1: Neutrino and antineutrino fluxes (thick curves) at production from a hidden source at 10 Mpc. The red (purple) thick solid curve corresponds to ν_μ (ν_e) flux while the red (purple) thick dashed curve corresponds to $\bar{\nu}_\mu$ ($\bar{\nu}_e$) flux. The labeled thin dot-dashed curves correspond to different components of the ν_μ flux.

2.4 Stellar envelope: density profile

The pre-explosion stars of the GRBs and the associated type Ic supernovae are widely believed to be He stars with radius $R_\star \approx 10^{11}$ cm. Supernovae of type II and Ib are thought to be explosions of larger stars with radius $R_\star \approx 3 \times 10^{12}$ cm, and have a H envelope on the He core. The envelopes usually have density profile $\rho(r) \propto r^{-k}$, with $k = 1.5 - 3$ [28]. Following Ref. [16] we adopt two stellar profiles, model [A] and [B] parameterized as

$$\begin{aligned}
 \text{[A]} \quad \rho(r) &= 3.3 \cdot 10^{-6} \text{ g cm}^{-3} \left(\frac{R_\star}{r} - 1 \right)^3, \\
 \text{[B]} \quad \rho(r) &= 2.8 \cdot 10^{-5} \text{ g cm}^{-3} \begin{cases} (R_\star/r)^{17/7}; & R_0 < r < r_b \\ (R_\star/r_b)^{17/7} (r - R_\star)^5 / (r_b - R_\star)^5; & r \geq r_b. \end{cases} \quad (2.10)
 \end{aligned}$$

The radius of inner border of the envelope equals $R_0 \approx r_j \approx 6.3 \cdot 10^{10}$ cm. According to Eq. (2.10), the density at R_0 is $\rho_0 \approx 0.33 \text{ g cm}^{-3}$ but can vary between (0.1–1) g cm^{-3} . The corresponding density of electrons is $n_0 = \rho_0 N_A Y_e \approx 10^{23} \text{ cm}^{-3}$ for $Y_e = 0.5$. Thus, neutrinos are produced in a low density region of jet and propagate through a higher density envelope. We assume that the boundary between the jet front and the envelope is sharp (much smaller than any oscillation scale). Neutrinos are produced in a low density region of jet. Typical size of this region is about $r_\nu \sim 6.3 \cdot 10^9$ cm, that is, about 1/10 of a jet size.

Notice that in general, all characteristics of a star change in time over jet duration. In particular, the jet parameters such as Γ_b and Δr_j are subject to variation over time.

The jet radius r_j is expected to increase slowly with time as the jet burrows through the envelope and eventually chokes or successfully breaks out, the parameters of the envelope $R_0 \approx r_j$ and n_0 change with time.

2.5 Neutrino fluxes and densities

According to Fig. 1 the flux integrated over the energy above 1 GeV, which gives approximately the total flux of neutrinos at r_j , is $F(> 1\text{GeV}) \approx 10^{30} \text{ cm}^{-2} \text{ s}^{-1}$. Then the number density of neutrinos in the source equals $n'_\nu \sim 10^{19} \text{ cm}^{-3}$. Notice that this is a density in the reference frame of the jet where neutrino emission is approximately isotropic. Therefore the potential due to $\nu - \nu$ scattering equals $\mu = \sqrt{2}G_F n'_\nu$. It should be compared with the vacuum frequency $\omega = \Delta m_{31}^2/2E'$. We find that $\mu \sim \omega$ at the energy $E' \sim 10^6 \text{ GeV}$, which corresponds to $E \sim 3 \cdot 10^6 \text{ GeV}$ in the observer frame. Consequently, for energies of interest the neutrino-neutrino effective potential is too small to induce the collective neutrino effects. Some collective effect may show up at $E > 1 \text{ PeV}$.

2.6 Coherence and averaging

Let us estimate the size of the wave packets of the produced neutrinos [18]. Pions mainly decay near shock fronts in the regions with strong magnetic field and increased density. Pions undergo collisions with surrounding photons and gas. The latter (gas) dominates at low energies ($E < 4 \cdot 10^2$) GeV. The mean free path with respect to the collisions can be estimated as $\lambda_{col} = (10^5, 3 \cdot 10^4, 5 \cdot 10^3) \text{ cm}$ for energies $E = (0.1, 1, 10) \text{ TeV}$, correspondingly (in the rest frame of jet bulk). For neutrino emission in the forward direction the size of the wave packet is then [18] $\sigma_x = \lambda_{col}/\gamma_\pi$, where γ_π is the Lorentz factor of pion. This gives $\sigma_x = (10^2, 3, 5 \cdot 10^{-2}) \text{ cm}$ for energies $E = (0.1, 1, 10) \text{ TeV}$, correspondingly. However, very strong kinematical shortening of the wave packets occur in presence of the magnetic field due to bending of pion trajectory. According to [18], the size of the wave packet is given by

$$\sigma_x = 3.5 \cdot 10^{-14} \text{ cm} \left(\frac{\Gamma_b 10^8 \text{ G}}{3 B} \right)^{1/2} \left(\frac{1 \text{ TeV}}{E} \right)^{3/2}. \quad (2.11)$$

For $\Gamma_b = 3$, $B = 10^8 \text{ G}$ and neutrino energies $E = (10^2, 10^3, 10^4) \text{ GeV}$ we obtain from this formula $\sigma_x = (10^{-12}, 3.5 \cdot 10^{-14}, 10^{-15}) \text{ cm}$ correspondingly.

Separation of the wave packets of different mass states on the way L is given by $d_s = L\Delta m^2/(2E^2)$. For typical distance 10 Mpc and Δm_{31}^2 we find

$$d_s = 0.045 \text{ cm} \left(\frac{1 \text{ TeV}}{E} \right)^2.$$

Thus, $d_s \gg \sigma_x$, and therefore the wave packets are well separated at the detection site. This means that the coherence is lost in configuration space in the course of neutrino propagation.

The coherence will not be restored at the detection. Indeed, the separated packets interact coherently, if the detector has long memory (time interval of coherent detection).

In this case the packets interactions would interfere and produce oscillatory pattern in the energy scale. The period of this oscillatory pattern, that is, the energy interval over which the phase changes by 2π is given by $\Delta E_T = El_\nu/L$, where l_ν is the oscillation length. For $L = 10$ Mpc and Δm_{31}^2 we obtain

$$\Delta E_T = 3 \cdot 10^{-3} \text{ eV} \left(\frac{E}{1\text{TeV}} \right)^2. \tag{2.12}$$

In practice it is not possible to determine the neutrino energy with such an accuracy. According to Eq. (2.12) at 1 TeV one needs to have the energy resolution $\Delta E/E < 10^{-15}$ to see non-averaged oscillation effect, whereas one may achieve $\Delta E/E \sim 0.1$. Thus, incoherent fluxes of mass eigenstates arrive at the surface of the Earth and interact in a detector.

Let us estimate the coherence length (the distance over which the wave packets are completely separated): $L_{coh} = \sigma_x 2E^2/\Delta m^2$. Using σ_x from (2.11) we obtain for $\Delta m_{31}^2 = 2.4 \cdot 10^{-3} \text{ eV}^2$

$$L_{coh} = 1.4 \cdot 10^{13} \text{ cm} \left(\frac{\Gamma_b 10^8 \text{ G}}{3 B} \right)^{1/2} \left(\frac{E}{1 \text{ TeV}} \right)^{1/2}.$$

Notice that $L_{coh} \propto \sqrt{E}$ and for $E > 200$ GeV, L_{coh} becomes larger than the size of star.

Some small part of pions decays in jet between shocks where the magnetic field is much smaller. For $B = 1$ G and $E = 1$ TeV we obtain $\sigma_x = 3.5 \cdot 10^{-10}$ cm and $L_{coh} = 1.4 \cdot 10^{17}$ cm. Similar situation is for the 2-body decay of K-mesons.

For muon decays (and also for 3-body K - decays) in the magnetic field, size of the neutrino wave packets is much larger [18]:

$$\sigma_x = 1.7 \cdot 10^{-11} \text{ cm} \left(\frac{\Gamma_b}{3} \right) \left(\frac{10^8 \text{ G}}{B} \right) \left(\frac{1 \text{ TeV}}{E} \right)^2.$$

For Δm_{31}^2 the coherence length equals

$$L_{coh} = 7 \cdot 10^{15} \text{ cm} \left(\frac{\Gamma_b}{3} \right) \left(\frac{10^8 \text{ G}}{B} \right),$$

and it does not depend on E . Although this length is about 2 - 3 orders larger than for pions, conclusions about loss of coherence are the same.

2.7 Effect of inelastic interactions

Evolution of the flavor neutrino states $\nu_f^T = (\nu_e, \nu_\mu, \nu_\tau)$ is described by the equation:

$$i \frac{d\nu_f}{dt} = (H + H_{int})\nu_f, \tag{2.13}$$

where H is the standard Hermitian part which includes the vacuum and refraction terms (the real part of scattering amplitudes, A^{Re}) and H_{int} describes inelastic interactions (the imaginary parts of scattering amplitudes, A^{Im}). Since the interactions are flavor diagonal in the lowest order of perturbation theory, we have

$$H_{int} \equiv -\frac{i}{2} \text{diag}(\Gamma_e, \Gamma_\mu, \Gamma_\tau).$$

For $E > 3 \cdot 10^3$ GeV (which corresponds to $0.5\Gamma = A^{Im} \sim A^{Re}$ for scattering on nucleons) the inelastic interaction can not be neglected. However, for such high energies in the first approximation the inelastic amplitudes for all neutrino species are the same: $\Gamma_e \approx \Gamma_\mu \approx \Gamma_\tau = \Gamma$. Indeed, the difference of masses of the charged leptons as well as the inelastic scattering on electrons can be neglected. Consequently, the inelastic part of the Hamiltonian becomes proportional to the unit matrix: $H_{int} = -\frac{i}{2}\Gamma I$. In this case the inelastic interactions and oscillations factor out. The former does not influence the oscillation pattern. Indeed, we can define new flavor wave functions as $\tilde{\nu}_f = e^{\Gamma t/2}\nu_f$. Inserting this relation into (2.13) we obtain

$$i\frac{d\tilde{\nu}_f}{dt} = H\tilde{\nu}_f$$

without the inelastic part. The factor due to inelastic interactions then appears in the probabilities: $P = e^{-\Gamma t}\tilde{P}$. This factor describes absorption of neutrinos or scattering which lead to departure of neutrinos from the coherent state. The effect of neutrino absorption in the charged current processes can be included in the energy spectrum of neutrinos. Decays of μ and τ produced in the CC interactions of neutrinos will generate secondary neutrinos. Due to falling down spectrum with energy, the contribution of these neutrinos to the total flux is small. In the case of neutral current neutrino interactions one should consider oscillations of the scattered neutrinos. In what follows we will neglect this scattering since the event rate of neutrinos with $E > 3 \cdot 10^3$ GeV is small even for the nearest plausible source.

3. Conversion inside the star: general consideration

3.1 Propagation basis

For the mixing matrix in vacuum, $\nu_f = U_{PMNS}\nu$, we use the standard parameterization

$$U_{PMNS} = U_{23}(\theta_{23})\Gamma_\delta U_{13}(\theta_{13})U_{12}(\theta_{12}), \tag{3.1}$$

where $U_{ij} = U(\theta_{ij})$ is the matrix of rotation in the ij -plane over the angle θ_{ij} and $\Gamma_\delta \equiv \text{diag}(0, 0, e^{i\delta})$. It is convenient to consider dynamics of the conversion in the so-called propagation basis, ν'_f , defined as

$$\nu_f \equiv U_{23}\Gamma_\delta\nu'_f, \quad \nu'_f \equiv (\nu_e, \nu'_\mu, \nu'_\tau). \tag{3.2}$$

In this basis the CP-phase is eliminated, so that the dynamics of conversion is not affected by δ . The CP-violation appears only in projection of the initial and final states onto the propagation basis. We have explicitly

$$U_{23}\Gamma_\delta = \begin{pmatrix} 1 & 0 & 0 \\ 0 & c_{23} & s_{23}e^{i\delta} \\ 0 & -s_{23} & c_{23}e^{i\delta} \end{pmatrix}, \tag{3.3}$$

where $s_{23} \equiv \sin \theta_{23}$, $c_{23} \equiv \cos \theta_{23}$. According to (3.1) and (3.2) the vacuum mixing matrix in the propagation basis is given by $\nu'_f = U'\nu$, where

$$U' = U_{13}U_{12} = \begin{pmatrix} c_{13}c_{12} & c_{13}s_{12} & s_{13} \\ -s_{12} & c_{12} & 0 \\ -s_{13}c_{12} & -s_{13}s_{12} & c_{13} \end{pmatrix}. \quad (3.4)$$

Here $c_{12} \equiv \cos \theta_{12}$, $s_{12} \equiv \sin \theta_{12}$, etc. It is straightforward to show that the mixing matrix in matter in the propagation basis, U'_m , up to additional small 2-3 rotation has the same form as in (3.4) with mixing angles in matter: $\theta_{12} \rightarrow \theta_{12}^m$, $\theta_{13} \rightarrow \theta_{13}^m$:

$$U'_m \approx \begin{pmatrix} c_{13}^m c_{12}^m & c_{13}^m s_{12}^m & s_{13}^m \\ -s_{12}^m & c_{12}^m & 0 \\ -s_{13}^m c_{12}^m & -s_{13}^m s_{12}^m & c_{13}^m \end{pmatrix}. \quad (3.5)$$

The level crossing scheme (see Fig. 2) is similar to the one for low energy supernova neutrinos (see, e.g., [32]).

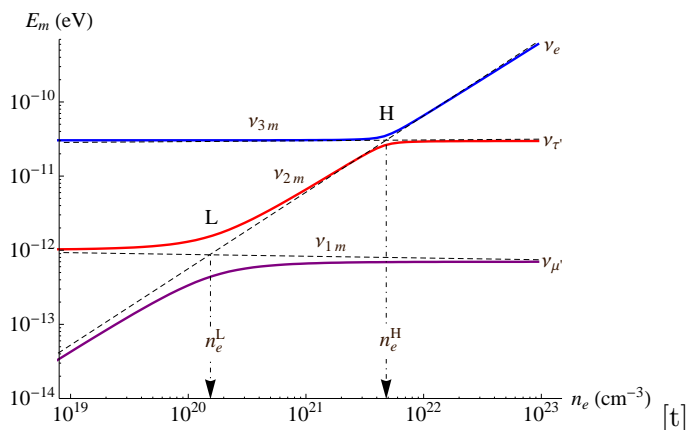


Figure 2: The level crossing scheme for neutrinos in stellar envelope in the case of normal mass hierarchy. The solid lines correspond to the eigenvalues of the effective Hamiltonian as functions of the electron number density. The dashed lines correspond to the energy levels of the flavor states ν_e , $\nu_{\mu'}$ and $\nu_{\tau'}$ in the propagation basis. The vertical dot-dashed lines indicate the L- and H- resonance densities. Note that the positions of the resonances are inversely proportional to the neutrino energy E (plotted here for $E = 2$ TeV). We used $\sin^2 2\theta_{13} = 0.08$.

3.2 General expressions for probabilities

Decays of π^- , μ^- and K^- mesons produce incoherent neutrino and antineutrino fluxes of definite flavors: ν_e , ν_{μ} , etc.. Since the mass states are the eigenstates of propagation in vacuum and coherence between them is lost due to separation of the corresponding wave packets (see Sec. 2.6), we can write for the $\nu_{\alpha} \rightarrow \nu_{\beta}$ conversion probability at the Earth

$$P(\nu_{\alpha} \rightarrow \nu_{\beta}) = \sum_i P_*(\nu_{\alpha} \rightarrow \nu_i) |U_{\beta i}|^2, \quad (3.6)$$

where $P_*(\nu_\alpha \rightarrow \nu_i)$ is the flavor-to-mass conversion probability inside the star. This expression differs from the one used in Ref. [16], and detailed explanation of the difference is given in the Appendix B. If neutrinos cross the Earth the formula (3.6) is modified as

$$P(\nu_\alpha \rightarrow \nu_\beta) = \sum_i P_*(\nu_\alpha \rightarrow \nu_i) P_E(\nu_i \rightarrow \nu_\beta), \quad (3.7)$$

where $P_E(\nu_i \rightarrow \nu_\beta)$ is the probability of $(\nu_i \rightarrow \nu_\beta)$ oscillations in the matter of the Earth. The probability P_E can substantially deviate from $|U_{\beta i}|^2$ at energies $E < 10$ GeV. For higher energies matter suppresses oscillations inside the Earth, so that the probability is reduced to the one in Eq. (3.6). We give explicit expressions for the probabilities in the Earth for constant density in Appendix C.

Inside a star the flavor conversion occurs first in jet and then in envelope. Therefore one should take into account oscillations in the production region of jet and perform integration over this region. Then the total conversion probability inside the star equals

$$P_*(\nu_\alpha \rightarrow \nu_i) = \frac{1}{r_\nu} \int_0^{r_\nu} dx \left| \sum_\xi A_{jet}(\nu_\alpha \rightarrow \nu_\xi)(x) \cdot A_{env}(\nu_\xi \rightarrow \nu_i) \right|^2,$$

where $A_{jet}(\nu_\alpha \rightarrow \nu_\xi)(x)$ is the amplitude of probability of ν_α transition to the flavor state ν_ξ inside jet: between the production point x and the inner border of the envelope. The integration is performed over the production region and in what follows we will use the one-dimensional (1D) integration for simplicity. Note that 1D consideration is valid if we consider neutrinos from a given source, although in this case the density profile can differ from the one in radial direction (recall that jet has rather large cone angle). If $\theta_{tr} \gtrsim \theta_{jet}$ is the angle between the radial (jet) direction and direction to observer, the radial distance equals $r = x \cos \theta_{tr}$, where x is the distance along the trajectory. Then the density profile which neutrino experiences is $n(x \cos \theta_{tr}) = n_0(x \cos \theta_{tr}/r_0)^{-k}$. In this case the density profile is flatter and the evolution will be more adiabatic. For neutrinos produced by all hidden sources (the diffuse flux) we need to perform also integration over $\cos \theta_{tr}$.

In the propagation basis the probability can be written as

$$P_*(\nu_\alpha \rightarrow \nu_i) = \frac{1}{r_\nu} \int_0^{r_\nu} dx \left| \sum_\xi \sum_\beta (U_{23} \Gamma_\delta)_{\alpha\beta} \cdot A_{jet}(\nu'_\beta \rightarrow \nu'_\xi)(x) \cdot A_{env}(\nu'_\xi \rightarrow \nu_i) \right|^2. \quad (3.8)$$

Here $A_{jet}(\nu'_\beta \rightarrow \nu'_\xi)$ is the amplitude of transition inside jet in the propagation basis. The probability averaged over the production region equals

$$P_*(\nu_\alpha \rightarrow \nu_i) = \frac{1}{r_\nu} \int_0^{r_\nu} dx |S_{i\alpha}|^2,$$

where $S_{i\alpha} \equiv A_*(\nu_\alpha \rightarrow \nu_i)$. The matrix of total flavor-to-flavor probabilities equals

$$\hat{P}_{tot} = \hat{P}_* \hat{P}_E, \quad (3.9)$$

or if there is no Earth matter effect:

$$\hat{P}_{tot} = \hat{P}_* \cdot P_{PMNS}^T, \quad (3.10)$$

where $P_{PMNS} \equiv || |(U_{PMNS})_{ij}|^2 ||$ is the matrix of moduli square of the mixing matrix elements in vacuum.

According to (3.8) the amplitudes of transitions inside the star is given by

$$A_*(\nu_\alpha \rightarrow \nu_i) = (U_{23}\Gamma_\delta)_{\alpha\beta} A_{jet}(\nu'_\beta \rightarrow \nu'_\xi) A_{env}(\nu'_\xi \rightarrow \nu_i).$$

In matrix form we have

$$S_* = (U_{23}\Gamma_\delta) S_{jet} S_{env}. \quad (3.11)$$

Here

$$(S_{jet})_{\xi\beta} \equiv A_{jet}(\nu'_\beta \rightarrow \nu'_\xi) \quad \text{and} \quad (S_{env})_{i\xi} \equiv A_{env}(\nu'_\xi \rightarrow \nu_i)$$

are the evolution matrices inside jet and inside an envelope in the propagation basis correspondingly.

For $E > 2 \cdot 10^3$ GeV or/and smaller production region the phase of oscillations inside jet is small and these oscillations can be neglected. Furthermore, as we will show in Sec. 4.5, the effect of oscillations inside jet is zero or small and so in the first approximation can be neglected. Therefore we will first consider oscillations inside the star ignoring oscillations inside jet. In this case $S_{jet} = I$ and $S_* \approx (U_{23}\Gamma_\delta) S_{env}$.

3.3 Matter affected range

In Fig. 3 we show the conversion probabilities in different channels for two different initial densities in the envelope. There are two key energies in the problem: the two resonance energies which correspond to maximal electron density in the envelope n_0 (density at the border between jet and envelope) ¹:

$$E_R^L \approx \frac{\Delta m_{21}^2}{2V_0} \cos 2\theta_{12}, \quad E_R^H \approx \frac{\Delta m_{31}^2}{2V_0} \cos 2\theta_{13},$$

where $V_0 = \sqrt{2} G_F n_0$. For $n_0 = 10^{23} \text{ cm}^{-3}$ we find

$$E_R^L = 1.3 \text{ GeV}, \quad E_R^H = 75 \text{ GeV}.$$

These energies determine the borders of energy regions with different dynamics of flavor conversion (see Fig. 3) inside the star:

1. $E < E_R^L$ - the vacuum oscillations (VO) region: VO dominate for both 1-2 and 1-3 modes.
2. $E_R^L \lesssim E \lesssim E_R^H$ - the intermediate energy range, (7 – 70) GeV. The corresponding neutrinos are produced between the two resonances. The 1-3 mixing and split lead to averaged vacuum oscillations (the mass eigenstate ν_3 decouples from the rest of system), whereas for 1-2 mixing and mass split the matter effects dominate.
3. $E_R^H \lesssim E \lesssim E_{na}$, where E_{na} is the energy of strong adiabaticity breaking. Neutrinos are produced above the 1-3 resonance in the density scale; here matter effects are important for both mixings. For the power dependence of the spectrum we have $E_{na} \sim R_* \Delta m_{31}^2 / 4\pi \sim 10^2 E_R^H$.

¹This is 2ν - definition, in fact there is some small shift of the 1-2 resonance due to 1-3 mixing.

4. $E > E_{na}$ - matter suppresses oscillations inside the star, here the flavor conversion is due to oscillations in vacuum from the surface of a star to the earth. Loss of coherence leads to the averaged oscillation result.

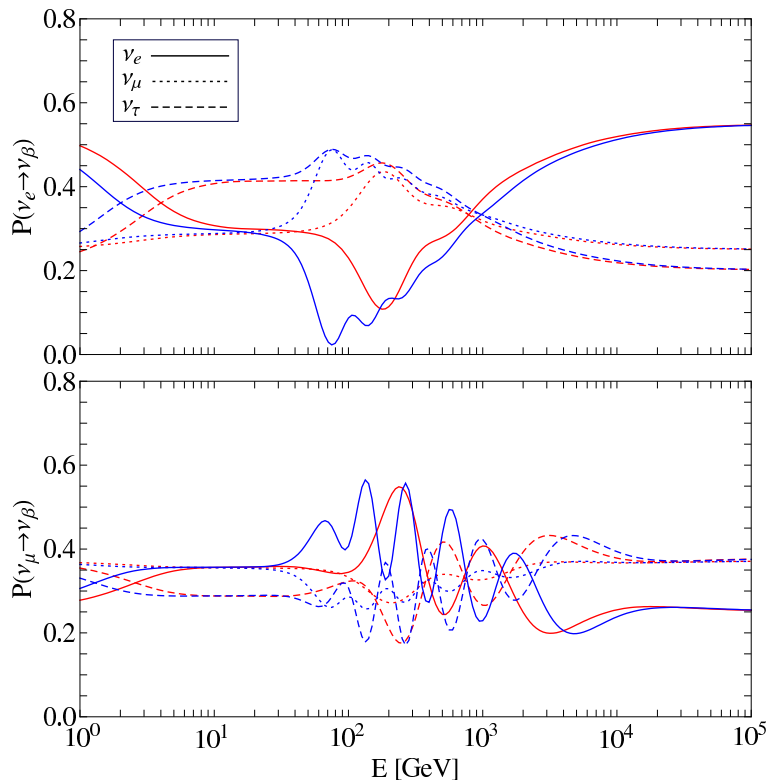


Figure 3: Probabilities of the $\nu_e \rightarrow \nu_\beta$ (top panel) and $\nu_\mu \rightarrow \nu_\beta$ (bottom panel) transitions for the density profile A with two different inner densities $n_0 = 10^{23} \text{ cm}^{-3}$ (red lines) and $n_0 = 2 \cdot 10^{23} \text{ cm}^{-3}$ (blue lines). We used $\sin^2 2\theta_{13} = 0.08$, $\sin^2 \theta_{23} = 0.5$, $\delta_{cp} = 0$ and normal mass hierarchy.

The matter affected range spans over 5 orders of magnitude from about 0.3 GeV to $3 \cdot 10^4$ GeV. With increase of n_0 the range expands in both directions.² According to Fig. 3 generic features of the energy dependences of the probabilities can be summarized as follows.

- Plateau in the intermediate range above the vacuum-to-matter transition region at (0.3 - 3) GeV.
- Peak or dip (depending on channel) at $E \gtrsim E_R^H$ due to the 1-3 resonance.
- Wiggles at $E \gtrsim E_R^H$ in the nonadiabatic edge, above the peak (dip). As we will show the wiggles are due to interference induced by adiabaticity breaking.

²Here we discuss whole energy affected range and discuss relevant physics in spite of the fact that the present detectors have rather high energy threshold $E \gtrsim 10^2$ GeV. Future experimental developments may, in principle, substantially reduce this threshold.

- The wiggles are different in channels with initial ν_e and ν_μ . According to Fig. 3 the wiggles are small in $\nu_e \rightarrow \nu_\beta$ channels (upper panel), and large in $\nu_\mu \rightarrow \nu_\beta$ channels.
- The wiggles modulate the non-adiabatic edge of the energy profile of the effect.

Note that the $\nu_e \rightarrow \nu_e$ probability as function of energy can be viewed as two dips in the energy profile, one embedded into another, which corresponds to crossing of two resonances: due to the 1-2 and 1-3 mixings. If the 1-3 mixing is small or zero, the 1-3 dip is absent and the plateau extends to higher energies. With further increase of energies the probabilities will converge without wiggles to the asymptotic values as in the case of solar neutrinos. In what follows we will explain these features.

3.4 Asymptotic values of probabilities

Outside the matter affected region the probabilities converge to the asymptotic values which are given by the averaged vacuum oscillation probabilities. Indeed, for $E \ll E_R^L$ the matter effects can be neglected and we deal with vacuum oscillations inside the star, (essentially the flavor state is projected onto mass eigenstates in the production region and then these eigenstates propagate inside the star without changes), so

$$P_*(\nu_\alpha \rightarrow \nu_i) = |U_{\alpha i}|^2, \tag{3.12}$$

and therefore Eq. (3.6) becomes

$$P(\nu_\alpha \rightarrow \nu_\beta) = \sum_i |U_{\alpha i}|^2 |U_{\beta i}|^2. \tag{3.13}$$

The same result (3.12), (3.13) are valid for very high energies: $E \gg E_R^H$. In this region matter suppresses oscillations inside the star. In other terms, for very high energies the adiabaticity is strongly broken and no flavor conversion occurs, $P_* = I$. Here we project ν_α onto mass eigenstates at the surface of the star, which is equivalent to the coherence lost. Again $P_*(\nu_\alpha \rightarrow \nu_i)$ equals (3.12) and the total probability is given by (3.13). The probabilities reach the asymptotic at $E \sim 10^5$ GeV and converge to the same asymptotic values below 1 GeV (in this sense the picture is symmetric) as in Fig. 3.

Since for antineutrinos in vacuum $U_{\alpha i} \rightarrow U_{\alpha i}^*$, the result (3.13) is also valid for antineutrinos: $P(\bar{\nu}_\alpha \rightarrow \bar{\nu}_\beta) = P(\nu_\alpha \rightarrow \nu_\beta)$. There is no CP-asymmetry, although the probabilities depend on the phase δ . Since the asymptotics does not depend on Δm^2 , for the inverted mass hierarchy we have again the same result (3.13).

3.5 Adiabatic conversion

At low energies ($E \lesssim E_R^H \sim 100$ GeV) the adiabaticity condition is satisfied and we can use results in the adiabatic approximation. Let ν_m^0 be the eigenstates of the Hamiltonian in the initial moment (at the inner border of the envelope). Then the flavor states can be represented in terms of ν_m^0 as $\nu_f = U_m^0 \nu_m^0$. The adiabatic evolution means that the transitions between the eigenstates can be neglected and therefore $\nu_m^0 \rightarrow \nu$, or explicitly

$$\begin{pmatrix} \nu_{1m}^0 \\ \nu_{2m}^0 \\ \nu_{3m}^0 \end{pmatrix} \rightarrow \begin{pmatrix} \nu_1 \\ \nu_2 \\ \nu_3 \end{pmatrix}. \tag{3.14}$$

Consequently, inside the star the flavor state ν_α evolves as $\nu_\alpha \rightarrow U_{\alpha i}^0 \nu_i$, and therefore the adiabatic probability is given by

$$P_*(\nu_\alpha \rightarrow \nu_i) = |U_{\alpha i}^0|^2.$$

Then the flavor transition probability at the Earth equals

$$P(\nu_\alpha \rightarrow \nu_\beta) = |U_{\alpha i}^0|^2 |U_{\beta i}|^2.$$

Let us describe the adiabatic transitions in the propagation basis. Now $\nu'_f = U_m'^0 \nu_m^0$, where $U_m'^0$ is the mixing matrix in matter in the initial moment (at the density n_0). According to Eq. (3.2), the flavor states can be written as $\nu_f = (U_{23}\Gamma_\delta)S_{jet}U_m'^0 \nu_m^0$. Therefore according to (3.14) $S\nu_f = (U_{23}\Gamma_\delta)S_{jet}U_m'^0 \nu$, and

$$S_* = \langle \nu | S | \nu_f \rangle = (U_{23}\Gamma_\delta)S_{jet}U_m'^0.$$

Neglecting oscillations inside jet we have $S_{jet} = I$ and

$$S_* = \langle \nu | S | \nu_f \rangle = (U_{23}\Gamma_\delta)U_m'^0. \tag{3.15}$$

The expression in (3.15) coincides with the mixing matrix in matter in the initial moment: $U_{\alpha i}^0 \approx (U_{23}\Gamma_\delta)U_m'^0$.

The adiabaticity condition can be satisfied at low energies, in particular, in the intermediate region. This region corresponds to neutrino production above the 1-2 resonance density. Far above the 1-2 resonance $\theta_{12}^m \approx \pi/2$. Therefore using Eq. (3.5) we obtain the mixing matrix in the initial state

$$U_m'^0 \approx \begin{pmatrix} 0 & c_{13}^0 & s_{13}^0 \\ -1 & 0 & 0 \\ 0 & -s_{13}^0 & c_{13}^0 \end{pmatrix}, \tag{3.16}$$

where c_{13}^0 and s_{13}^0 are the mixing parameters in the initial moment. Inserting this matrix into Eq. (3.15) we obtain the matrix of amplitudes

$$S_* \approx U_{\alpha i}^0 = \begin{pmatrix} 0 & c_{13}^0 & s_{13}^0 \\ -c_{23} & -s_{13}^0 s_{23} e^{i\delta} & c_{13}^0 s_{23} e^{i\delta} \\ +s_{23} & -s_{13}^0 c_{23} e^{i\delta} & -c_{13}^0 c_{23} e^{i\delta} \end{pmatrix}. \tag{3.17}$$

Consequently, the matrix of probabilities inside the star equals

$$\hat{P}_* \approx \begin{pmatrix} 0 & c_{13}^{0\ 2} & s_{13}^{0\ 2} \\ c_{23}^2 & s_{13}^{0\ 2} s_{23}^2 & c_{13}^{0\ 2} s_{23}^2 \\ s_{23}^2 & s_{13}^{0\ 2} c_{23}^2 & c_{13}^{0\ 2} c_{23}^2 \end{pmatrix}, \tag{3.18}$$

where the rows correspond to the initial flavor states ν_e, ν_μ, ν_τ and the columns correspond to the final mass states. According to (3.18), the probabilities do not depend on δ and this is the consequence of the adiabatic propagation at the energies above the 1-2 resonance. So, any dependence on δ is manifestation of the adiabaticity violation or/and closeness to

the 1-2 resonance. The flavor transition probabilities at the detector are then given by Eq. (3.10). Some dependence on δ follows from dependence of the projections of the mass states to flavor states back at the detection, i.e., from factors $|U_{PMNS}|^2$ as we will discuss in Sec. 4.6.

Let us consider some particular cases of Eq. (3.18).

1. In the intermediate range (plateau) we have $\theta_{13}^0 \approx \theta_{13}$ and the probability matrix becomes

$$\hat{P}_* \approx \begin{pmatrix} 0 & c_{13}^2 & s_{13}^2 \\ c_{23}^2 & s_{13}^2 s_{23}^2 & c_{13}^2 s_{23}^2 \\ s_{23}^2 & s_{13}^2 c_{23}^2 & c_{13}^2 c_{23}^2 \end{pmatrix}. \quad (3.19)$$

2. Above the H-resonance, $E \gtrsim E_R^H$, we have $\theta_{13}^0 \approx \pi/2$, so that $c_{13}^0 \approx 0$ and $s_{13}^0 \approx 1$, and consequently,

$$U_m^0 \approx \begin{pmatrix} 0 & 0 & 1 \\ -1 & 0 & 0 \\ 0 & -1 & 0 \end{pmatrix}.$$

For large enough θ_{13} the adiabaticity is fulfilled, and using the adiabatic result (3.15) we obtain

$$S_* \approx \begin{pmatrix} 0 & 0 & 1 \\ -c_{23} & -s_{23}e^{i\delta} & 0 \\ s_{23} & -c_{23}e^{i\delta} & 0 \end{pmatrix}$$

which leads to

$$\hat{P}_* \approx \begin{pmatrix} 0 & 0 & 1 \\ c_{23}^2 & s_{23}^2 & 0 \\ s_{23}^2 & c_{23}^2 & 0 \end{pmatrix}. \quad (3.20)$$

Then, according to general formula (3.10) the flavor probability matrix equals

$$\hat{P} \approx \begin{pmatrix} |U_{e3}|^2 & |U_{\mu3}|^2 & |U_{\tau3}|^2 \\ c_{23}^2|U_{e1}|^2 + s_{23}^2|U_{e2}|^2 & c_{23}^2|U_{\mu1}|^2 + s_{23}^2|U_{\mu2}|^2 & c_{23}^2|U_{\tau1}|^2 + s_{23}^2|U_{\tau2}|^2 \\ s_{23}^2|U_{e1}|^2 + c_{23}^2|U_{e2}|^2 & s_{23}^2|U_{\mu1}|^2 + c_{23}^2|U_{\mu2}|^2 & s_{23}^2|U_{\tau1}|^2 + c_{23}^2|U_{\tau2}|^2 \end{pmatrix}. \quad (3.21)$$

3. For antineutrinos, the 1-2 mixing is suppressed at $E \gtrsim E_R^L$, so that $\theta_{12}^0 \approx 0$. Therefore, according to (3.5) we obtain

$$\bar{U}_m^0 \approx \begin{pmatrix} c_{13}^0 & 0 & s_{13}^0 \\ 0 & 1 & 0 \\ -s_{13}^0 & 0 & c_{13}^0 \end{pmatrix}.$$

The matrix of amplitudes in the flavor basis equals $\bar{S}_* = (U_{23}\Gamma_{-\delta})\bar{U}_m^0$, or explicitly

$$\bar{S}_* \approx \begin{pmatrix} c_{13}^0 & 0 & s_{13}^0 \\ -s_{13}^0 s_{23} e^{-i\delta} & c_{23} & c_{13}^0 s_{23} e^{-i\delta} \\ -s_{13}^0 c_{23} e^{-i\delta} & s_{23} & c_{13}^0 c_{23} e^{-i\delta} \end{pmatrix}.$$

Consequently, the matrix of probabilities inside the star is

$$\hat{P}_* \approx \begin{pmatrix} c_{13}^0{}^2 & 0 & s_{13}^0{}^2 \\ s_{13}^0{}^2 c_{23}^2 & c_{23}^2 & c_{13}^0{}^2 s_{23}^2 \\ s_{13}^0{}^2 c_{23}^2 & s_{23}^2 & c_{13}^0{}^2 c_{23}^2 \end{pmatrix}. \quad (3.22)$$

4. For the inverted mass hierarchy (IH) above the 1-2 resonance we have the same initial mixing matrix as for the normal mass hierarchy (NH) given in Eq. (3.16), the same S-matrix (3.17) and the same matrix of probabilities (3.18).

In the intermediate energy range (below 1-3 resonance) the 1-3 mixing equals approximately the vacuum mixing as in NH case and therefore the probability matrix is as in Eq. (3.19). The difference appears at higher energies, since there the matter effect on 1-3 mixing is different for the normal and inverted hierarchies. In particular, above the 1-3 resonance we have in the case of IH: $\theta_{13}^0 \approx 0$, $c_{13}^0 \approx 1$, $s_{13}^0 \approx 0$ and

$$\hat{P}_* \approx \begin{pmatrix} 0 & 1 & 0 \\ c_{23}^2 & 0 & s_{23}^2 \\ s_{23}^2 & 0 & c_{23}^2 \end{pmatrix}. \quad (3.23)$$

Then the matrix of flavor transition probabilities in case of IH becomes

$$\hat{P} \approx \begin{pmatrix} |U_{e2}|^2 & |U_{\mu 2}|^2 & |U_{\tau 2}|^2 \\ c_{23}^2 |U_{e1}|^2 + s_{23}^2 |U_{e3}|^2 & c_{23}^2 |U_{\mu 1}|^2 + s_{23}^2 |U_{\mu 3}|^2 & c_{23}^2 |U_{\tau 1}|^2 + s_{23}^2 |U_{\tau 3}|^2 \\ s_{23}^2 |U_{e1}|^2 + c_{23}^2 |U_{e3}|^2 & s_{23}^2 |U_{\mu 1}|^2 + c_{23}^2 |U_{\mu 3}|^2 & s_{23}^2 |U_{\tau 1}|^2 + c_{23}^2 |U_{\tau 3}|^2 \end{pmatrix},$$

as compared to the NH case (3.21).

For antineutrinos, the situation is similar: in the intermediate region the results coincide with those for NH, whereas above the H-resonance energy the results change. Now this is the resonance channel and $c_{13}^0 \approx 0$, $s_{13}^0 \approx 1$. Consequently, the matrix of probabilities of the flavor to mass transitions becomes:

$$\hat{P}_* \approx \begin{pmatrix} 0 & 0 & 1 \\ s_{23}^2 & c_{23}^2 & 0 \\ c_{23}^2 & s_{23}^2 & 0 \end{pmatrix}. \quad (3.24)$$

3.6 Adiabaticity breaking

At high energies, not far above the H-resonance for the profiles A and B, the adiabaticity is broken and in contrast to Eq. (3.14) the transitions between the eigenstates of propagation in matter occur. The adiabaticity is broken mainly in resonance regions, so that in resonances jumps from one eigenstate to another occur.

We will consider evolution in the so-called factorization approximation when two level crossings (1-3 and 1-2) occur independently one after another and do not influence each other (see Fig. 2). Probability of crossing of two resonances equals the product probabilities of crossings of individual resonances.

The ‘‘jump’’ transition probability in each crossing is well described by the double exponent formula [33]

$$P_{jump} = \frac{e^{2\pi\lambda_n\omega(1-\sin^2\theta)} - 1}{e^{2\pi\lambda_n\omega} - 1}, \quad (3.25)$$

where $\omega \equiv \Delta m^2/2E$ and $\lambda_n \equiv n/(dn/dr)$ is the scale of the electron density change. For 1-3 level crossing the jump probability $P_H = P_{jump}(\Delta m_{31}^2, \theta_{13})$ and for the 1-2 level crossing the jump probability $P_L(\Delta m_{21}^2, \theta_{12})$ (see Fig. 2). In Fig. 4 we show the jump probabilities computed for different neutrino parameters.

Let us consider ν_e production with energies substantially larger than the resonance energy, so that in initial state $\nu_e \approx \nu_{3m}$. In factorization approximation we have

$$P_*(\nu_e \rightarrow \nu_1) = P_H P_L, \quad P_*(\nu_e \rightarrow \nu_2) = P_H(1 - P_L), \quad P_*(\nu_e \rightarrow \nu_3) = 1 - P_H. \quad (3.26)$$

Then the $(\nu_e \rightarrow \nu_e)$ probability equals

$$P(\nu_e \rightarrow \nu_e) = (1 - P_H)|U_{e3}|^2 + P_H(1 - P_L)|U_{e2}|^2 + P_H P_L |U_{e1}|^2.$$

It can be rewritten as

$$P(\nu_e \rightarrow \nu_e) = |U_{e3}|^2 + P_H(|U_{e2}|^2 - |U_{e3}|^2) + P_H P_L (|U_{e1}|^2 - |U_{e2}|^2).$$

For other channels we have

$$P(\nu_e \rightarrow \nu_\mu) = (1 - P_H)|U_{\mu3}|^2 + P_H(1 - P_L)|U_{\mu2}|^2 + P_H P_L |U_{\mu1}|^2, \quad (3.27)$$

and similarly for transition to ν_τ .

The jump probabilities have the following asymptotics for $E \rightarrow \infty$:

$$P_H \rightarrow 1 - |U_{e3}|^2, \quad P_L \rightarrow \frac{|U_{e1}|^2}{1 - |U_{e3}|^2}. \quad (3.28)$$

Indeed, the limit $E \rightarrow \infty$ corresponds to absence of flavor transformation, i.e., $\nu_e \rightarrow \nu_e$. If the initial state is $\nu_e = \nu_{3m}$, the result for P_H is obtained in the 2ν - approximation neglecting matter effect on the 1-3 mixing in the intermediate point between the two resonances. Then the expression for P_L can be found from the condition that the 3ν - probability $P_*(\nu_e \rightarrow \nu_1) = |U_{e1}|^2$ (since $\nu_e \rightarrow \nu_e$), and therefore according to (3.26): $P_L = |U_{e1}|^2/P_H$. Finally, using asymptotic expression for P_H we arrive at the result shown in Eq. (3.28).

It is interesting to note that the adiabaticity is broken quite similarly in the same energy range for both resonances. This feature is the consequence of the fact that for $\sin^2 2\theta_{13} \sim 0.08$: $\sin^2 2\theta_{13} \Delta m_{31}^2 \sim \sin^2 2\theta_{12} \Delta m_{21}^2$.

Due to breaking of adiabaticity new interference effects emerge which lead to oscillatory behavior (“wiggles”) of the conversion probabilities (see Fig. 3). There are two types of the interference effects which are related to the adiabaticity violation in the H-resonance and L-resonance. We will call the results of these interferences the H-wiggles and the L-wiggles correspondingly. In general both L- and H- wiggles are present in all the channels simultaneously, however, as we will show in a given channel one type of wiggles dominates.

3.7 H-wiggles

The H-wiggles are related to mixing of the eigenstates ν_{2m} and ν_{3m} in a given flavor state and to the adiabaticity violation in the H-resonance. Above the H-resonance substantial admixture of ν_{2m} and ν_{3m} appear in the ν_e -state, and therefore the H-wiggles dominate in ν_e channels.

Let us neglect 1-2 mixing and consider transition $\nu_e \rightarrow \nu_{2m}$ in the region of H-resonance, i.e. compute the probability to find ν_{2m} at densities below the H-resonance but above

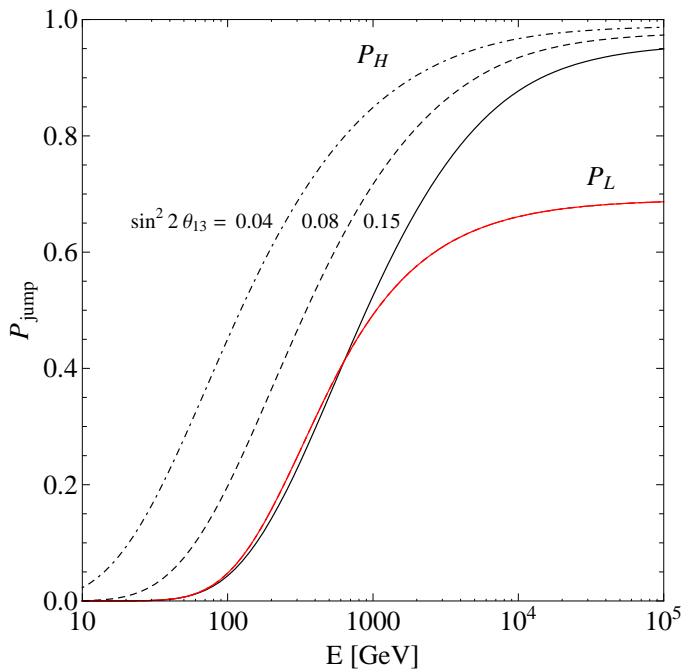


Figure 4: The jump probabilities in the H-resonance P_H (black lines) and in the L-resonance P_L (red line) as functions of neutrino energy. P_H is shown for three different values of $\sin^2 \theta_{13}$. We use the profile A and neutrino parameters: $\Delta m_{21}^2 = 8 \cdot 10^{-5} \text{ eV}^2$, $\Delta m_{31}^2 = 2.4 \cdot 10^{-3} \text{ eV}^2$, $\sin^2 2\theta_{12} = 0.86$.

the L-resonance. The problem is reduced to 2ν -problem according to the factorization approximation. In the H-resonance there are two channels of transition $\nu_e \rightarrow \nu_{2m}$:

$$\nu_e \rightarrow \nu_{2m} \rightarrow \nu_{2m}, \quad \nu_e \rightarrow \nu_{3m} \rightarrow \nu_{2m},$$

where the first arrow denotes projection of ν_e state on the corresponding eigenstate. It is the interference of the corresponding amplitudes that leads to the H-wiggles.

Let us quantify the interference picture. At the production point

$$\nu_e \approx \cos \theta_{13}^0 \nu_{2m} + \sin \theta_{13}^0 \nu_{3m}, \tag{3.29}$$

where θ_{13}^0 is the mixing angle in matter at the production point:

$$\sin^2 2\theta_{13}^0 \approx \frac{\sin^2 2\theta_{13}}{\cos^2 2\theta_{13}(1 - E/E_R^H)^2 + \sin^2 2\theta_{13}}.$$

Above the resonance, $E > E_R^H$, the angle $\theta_{13}^0 \rightarrow \pi/2$ and the admixture of ν_{2m} , given by $\cos \theta_{13}^0$, decreases. According to Eq. (3.29), below the H-resonance the total amplitude of probability to find ν_{2m} is given by

$$A(\nu_e \rightarrow \nu_{2m}) = \cos \theta_{13}^0 A_{22} + \sin \theta_{13}^0 A_{32},$$

where A_{32} is the amplitude of $\nu_{3m} \rightarrow \nu_{2m}$ transition in the H-resonance, $|A_{32}| = \sqrt{P_H}$, and $|A_{22}| = \sqrt{1 - P_H}$ is the amplitude of survival probability. Then the probability to find ν_{2m} equals

$$P(\nu_e \rightarrow \nu_{2m}) = \cos^2 \theta_{13}^0 (1 - P_H) + \sin^2 \theta_{13}^0 P_H - \sin 2\theta_{13}^0 \sqrt{P_H(1 - P_H)} \cos \phi_H, \quad (3.30)$$

where

$$\phi_H \equiv \text{Arg}(A_{22} A_{32}^*).$$

The last term in Eq. (3.30) is the interference term of two amplitudes which is responsible for the wiggles. The amplitude of wiggles is given by

$$W = \sin 2\theta_{13}^0 \sqrt{P_H(1 - P_H)}.$$

Using the formula (3.25) for P_H and for $\sin^2 \theta_{13} = 0.02$ we find the following values: $W = (0.05, 0.035, 0.025, 0.013)$, for $E = (200, 300, 500, 1000)$ GeV respectively; in agreement with results of the numerical computations in Fig. 3.

Let us estimate the phase ϕ_H . Note that transition between the eigenstates $\nu_{3m} \rightarrow \nu_{2m}$ is driven by the derivative $\dot{\theta}_{13}^m$ and occurs mainly in the resonance region $r_R \pm \Delta r_R$. Here $r_R = r_R(E)$ is determined from the resonance condition, $\sqrt{2}G_F n_e(r_R) = \Delta m_{31}^2/(2E)$, and the half-size of the resonance region is given by

$$\Delta r_R = \lambda_n \tan 2\theta_{13} = \frac{n}{dn/dr} \tan 2\theta_{13}.$$

For the power dependence of the density on distance,

$$n = n_0 \left(\frac{r}{R_0} \right)^{-k},$$

the scale factor equals $\lambda_n = r/k$. Therefore $\Delta r_R = r_R \tan 2\theta_{13}/k$.

The whole evolution of the phase ϕ can be divided into three parts: (i) from R_0 to $r_R - \Delta r_a$, where the system evolves adiabatically and transitions $\nu_{3m} \leftrightarrow \nu_{2m}$ can be neglected; (ii) from $r_R - \Delta r_a$ to $r_R + \Delta r_a$, where the transitions $\nu_{3m} \leftrightarrow \nu_{2m}$ occur; and (iii) from $r_R + \Delta r_a$ to R_* , where the adiabaticity is restored and states ν_{3m}, ν_{2m} evolve independently again. For moderate adiabaticity breaking $\Delta r_a \lesssim \Delta r_R$; for high energies the adiabaticity is broken even beyond the resonance layer.

The total amplitudes A_{22} and A_{32} introduced above can be written as $A_{22} = A_{22}^{iii} A_{22}^{ii} A_{22}^i$ and $A_{32} = A_{22}^{iii} A_{32}^{ii} A_{33}^i$ since $A_{32} \neq 0$ only in the region (ii). Note that the amplitudes in the region (ii) and consequently phases coincide for both A_{22} and A_{32} . Correspondingly, the total phases $\phi_2 \equiv \text{arg}(A_{22})$ and $\phi_3 \equiv \text{arg}(A_{32})$ equal

$$\phi_2 = \phi_2^{(i)} + \phi_2^{(ii)} + \phi_2^{(iii)}, \quad \phi_3 = \phi_3^{(i)} + \phi_3^{(ii)} + \phi_2^{(iii)}, \quad (3.31)$$

where $\phi_j^{(i)}$ and $\phi_j^{(iii)}$ ($j = 2, 3$) are the adiabatic phases in the regions (i) and (iii) correspondingly, whereas $\phi_2^{(ii)} \equiv \text{arg}(A_{22}^{(ii)})$ and $\phi_3^{(ii)} \equiv \text{arg}(A_{32}^{(ii)})$ are non-adiabatic phases.

Note that the last terms in Eqs. (3.31) (contributions from the region (iii)) are identical. Thus, the phase difference we are looking for equals:

$$\phi_H = \phi_3 - \phi_2 = \Delta\phi^{(i)} - \text{Arg}(A_{22}^{(ii)} A_{23}^{(ii)*}),$$

where $\Delta\phi^{(i)} \equiv \phi_3^{(i)} - \phi_2^{(i)}$ is the adiabatic phase difference acquired in the region (i):

$$\Delta\phi^{(i)} \approx \int_{R_0}^{r_R(E) - \Delta r_a(E)} dx \sqrt{\left[V(x) - \cos 2\theta_{13} \frac{\Delta m^2}{2E} \right]^2 + \sin^2 2\theta_{13} \left(\frac{\Delta m^2}{2E} \right)^2}. \quad (3.32)$$

For power-law density profile the upper limit of integration equals $r_R(E)(1 - \tan 2\theta_{13}/k)$.

Few comments are in order. The phase ϕ_H does not depend on evolution above (outside) the resonance (region (iii)) and therefore it does not depend on R_* . The phase depends on r_j via the adiabatic phase contribution. The non-adiabatic contribution $\text{Arg}[A_{22}^R A_{23}^{R*}] < 2\pi$ (or much smaller) since the adiabaticity violation corresponds to the width of the resonance layer to be smaller than the oscillation length. To a good approximation the phase in region (ii) can be taken into account by extending the integral in Eq. (3.32) to this region, that is, taking $r_R(E) + \Delta r_a(E)$ as the upper limit of integration.

If $V \gg \Delta m^2/(2E)$, the adiabatic phase can be estimated in the following way:

$$\Delta\phi^{(i)} \approx \int_{R_0}^{r_R - \Delta r_R} V(x) dx - \frac{\Delta m^2}{2E} \cos 2\theta_{13} [r_R - \Delta r_R - R_0], \quad (3.33)$$

where we have taken $\Delta r_a = \Delta r_R$. This allows us also to estimate the period of wiggles in the energy scale. The first term in (3.33) only weakly depends on energy. This is because $V(x)$ is a steeply decreasing function of x (the power $k \approx 3$) and the integral is given mainly by the lower limit $V(R_0)$, which is independent of E . The upper limit depends on E but its contribution to $\Delta\phi^{(i)}$ is smaller than the second term in (3.33) and therefore will not change the period of wiggles substantially. Hence it is enough to study energy dependence of the second term which can be rewritten as

$$\phi_{ad}(E) \approx \frac{2\pi}{l_\nu} [r_R(E) - \Delta r_R(E) - R_0]. \quad (3.34)$$

This dependence on energy agrees well with periods of wiggles obtained from exact numerical computations (Fig. 3). The key point that the phase should be computed not down to R_* (which would introduce much faster oscillations) but down to $\sim r_R + \Delta r_a$.

The H-wiggles have not been observed in the probabilities for other objects. In the case of SMA solution of the solar neutrino problem, due to smallness of the vacuum mixing angle the wiggles are so small that they are simply unobservable. For the LOW solution the mixing at the production point is very strongly suppressed. For supernova neutrinos, again the amplitude of the wiggles is very strongly suppressed and, moreover, the period is so small that the wiggles are averaged out.

3.8 L-wiggles

The L-wiggles are the consequence of mixing of ν_{1m} and ν_{2m} in a given flavor state ν_α and the interference of the transition amplitudes

$$\nu_\alpha \rightarrow \nu_{1m} \rightarrow \nu_i \quad \text{and} \quad \nu_\alpha \rightarrow \nu_{2m} \rightarrow \nu_i, \quad (3.35)$$

where $i = 1, 2$. For energies above the H-resonance the states ν_{1m} and ν_{2m} are mixed mainly in ν_μ and ν_τ , and their admixture in ν_e is negligible. Therefore the L-wiggles are realized in channels with initial states of ν_μ and ν_τ . (see Fig. 3, upper panel). The transitions (3.35) appear due to adiabaticity violation in the L-resonance.

For definiteness we will describe the wiggles in the ν_μ channels in the case of normal mass hierarchy. According to (3.17) in the production point ν_μ has the following matter eigenstate content

$$\nu_\mu = -c_{23}\nu_{1m} - s_{13}^0 s_{23} e^{i\delta} \nu_{2m} + c_{13}^0 s_{23} e^{i\delta} \nu_{3m}. \quad (3.36)$$

Note that below the H-resonance energy the admixture of ν_{2m} is suppressed by smallness of $s_{13}^0 \approx s_{13}$. In contrast, for $E \gtrsim E_R^H$ we have $s_{13}^0 \approx 1$ and according to (3.36)

$$\nu_\mu \approx -c_{23}\nu_{1m} - s_{23} e^{i\delta} \nu_{2m}.$$

Consider evolution of this state. Its ν_{1m} and ν_{2m} components undergo various transformations with the following amplitudes in factorization approximation:

$$\begin{aligned} |A(\nu_{1m} \rightarrow \nu_2)| &= \sqrt{P_L}, & |A(\nu_{2m} \rightarrow \nu_{2m} \rightarrow \nu_2)| &= \sqrt{(1 - P_H)(1 - P_L)}, \\ |A(\nu_{1m} \rightarrow \nu_1)| &= \sqrt{1 - P_L}, & |A(\nu_{2m} \rightarrow \nu_{2m} \rightarrow \nu_1)| &= \sqrt{(1 - P_H)P_L}. \end{aligned}$$

Furthermore, at the resonance crossing $A(\nu_{1m} \rightarrow \nu_{2m}) = -A(\nu_{2m} \rightarrow \nu_{1m})$. (For completeness: $|A(\nu_{2m} \rightarrow \nu_3)| = \sqrt{P_H}$, which is irrelevant for this interference.) Note that ν_{1m} crosses only L-resonance, whereas ν_{2m} crosses both resonances which is indicated by two arrows. Summing up the amplitudes from different channels of transitions we obtain

$$\begin{aligned} P_*(\nu_\mu \rightarrow \nu_1) &= \left| c_{23} \sqrt{1 - P_L} - e^{-i\phi_L} s_{23} e^{i\delta} \sqrt{(1 - P_H)P_L} \right|^2, \\ P_*(\nu_\mu \rightarrow \nu_2) &= \left| c_{23} \sqrt{P_L} + e^{-i\phi_\mu} s_{23} e^{i\delta} \sqrt{(1 - P_H)(1 - P_L)} \right|^2, \\ P_*(\nu_\mu \rightarrow \nu_3) &= \sin^2 \theta_{23} P_H. \end{aligned} \quad (3.37)$$

Here ϕ_L is the phase difference of the amplitudes collected from the production point to the end of L-resonance region where the adiabaticity is restored. To a good approximation one can use for ϕ_L the adiabatic phase difference:

$$\phi_L \approx \int_{R_0}^{r_R^L + \Delta r_R^L} dx (H_{2m} - H_{1m}). \quad (3.38)$$

The probabilities (3.37) can be rewritten as

$$\begin{aligned} P_*(\nu_\mu \rightarrow \nu_1) &= c_{23}^2 (1 - P_L) + s_{23}^2 (1 - P_H) P_L - I_\mu, \\ P_*(\nu_\mu \rightarrow \nu_2) &= c_{23}^2 P_L + s_{23}^2 (1 - P_H) (1 - P_L) + I_\mu, \\ P_*(\nu_\mu \rightarrow \nu_3) &= s_{23}^2 P_H, \end{aligned} \quad (3.39)$$

where the interference term equals

$$I_\mu \equiv \sin 2\theta_{23} \cos(\phi_L + \delta) \sqrt{(1 - P_H)P_L(1 - P_L)}. \quad (3.40)$$

Note that the CP-violation phase enters together with the oscillation (“strong” phase) and to disentangle the former one needs to know ϕ_L . Let us first summarize properties of the interference term.

1. The interference term is not suppressed by small mixing in contrast to the H-wiggles considered in the previous section. Here the admixture is determined by the vacuum mixing angle θ_{23} which is close to maximal. In fact, in the energy range where $P_L \sim 1/2$, this term can have the amplitude of the order 1.
2. The interference term appears in the transitions to ν_1 and ν_2 and not to ν_3 . It has an opposite sign in $\nu_\mu \rightarrow \nu_1$ and $\nu_\mu \rightarrow \nu_2$ probabilities (as it should be according to unitarity).
3. The interference term vanishes if $P_H = 1$ which, in turn, is realized for $\theta_{13} \rightarrow 0$. Non-zero 1-3 mixing is a necessary condition for its appearance. The amplitude is maximal if the transition in H-resonance is adiabatic. With increase of energy the adiabaticity in H-resonance is broken, $P_H \rightarrow 1$, and this suppresses the H-wiggles.
4. A necessary condition for appearance of wiggles are $P_L \neq 0$ and $P_L \neq 1$, that is, the adiabaticity should be broken in the L-resonance but it should not be broken very strongly.
5. The energy region where the L-wiggles are realized (more precisely, the lower border of this region) is determined by the following two conditions:

- the mixing of the eigenstates ν_{1m} and ν_{2m} should be large enough which happens in the region of the H-resonance and above it;
- the adiabaticity in the L-resonance should be broken. For the density profiles we are discussing the adiabaticity starts to be broken in the energy range of H-resonance and above it (which is to some extent accidental). As a result, the L-wiggles appear in the same energy region as the H-wiggles.

The flavor probabilities can be obtained plugging expressions (3.39) in (3.6). In particular,

$$P(\nu_\mu \rightarrow \nu_e) = \cos^2 \theta_{23} [|U_{e1}|^2 - P_L(|U_{e1}|^2 - |U_{e2}|^2)] + \sin^2 \theta_{23}(1 - P_H) [|U_{e2}|^2 + P_L(|U_{e1}|^2 - |U_{e2}|^2)] + (|U_{e2}|^2 - |U_{e1}|^2)I_\mu .$$

Let us consider separately the interference terms in the flavor probabilities. According to (3.39)

$$\begin{aligned} P(\nu_\mu \rightarrow \nu_e)_{int} &= (|U_{e2}|^2 - |U_{e1}|^2)I_\mu, \\ P(\nu_\mu \rightarrow \nu_\mu)_{int} &= (|U_{\mu 2}|^2 - |U_{\mu 1}|^2)I_\mu, \\ P(\nu_\mu \rightarrow \nu_\tau)_{int} &= (|U_{\tau 2}|^2 - |U_{\tau 1}|^2)I_\mu. \end{aligned}$$

For the selected values of the mixing angles $s_{23}^2 = 0.5$ and $\sin^2 2\theta_{13} = 0.08$ we have

$$P(\nu_\mu \rightarrow \nu_e)_{int} = -0.372I_\mu , \quad P(\nu_\mu \rightarrow \nu_\tau)_{int} = 0.318I_\mu , \quad P(\nu_\mu \rightarrow \nu_\mu)_{int} = 0.054 ,$$

in agreement with the results of numerical computations (see Fig. 3, lower panel). The wiggles in the $\nu_\mu \rightarrow \nu_e$ and $\nu_\mu \rightarrow \nu_\tau$ channels are large and in opposite phase and their

amplitude decreases with increase of energy because $P_L \rightarrow 1$ and $P_H \rightarrow 1$. The L-wiggles are suppressed in the $\nu_\mu \rightarrow \nu_\mu$ channel.

Let us now consider the phase of oscillatory behavior (3.38). The phase ϕ_L is collected (i) from the production point r_j to the H-resonance, r_R^H . Here the difference of eigenvalues is essentially given by the vacuum frequency: $\Delta m_{13}^2/2E$; (ii) in the H-resonance region and below: here the difference of eigenvalues start to decrease down to $\sim \Delta m_{12}^2/2E$; (iii) in the L-resonance, where the frequency is $\sim \Delta m_{12}^2/(2E \sin 2\theta_{12})$. The phases collected in regions (ii) and (iii) are small. In the L-resonance the oscillation length becomes larger than whole baseline. For instance for $E = 200$ GeV, we obtain $l_\nu \sim 6 \cdot 10^{11}$ cm $\gg r_R^L$. Although now the phase is collected from much larger region than in the case of H-wiggles: from r_j to $r_R^L + \Delta r_R^L$ (e.g. $2 \cdot 10^{11}$ cm, for $E \sim 200$ GeV), the phase ϕ_L is comparable to ϕ_H (collected by $0.7 \cdot 10^{11}$ cm). The reason is that the phase between $r_R^H + \Delta r_R^H$ and $r_R^L + \Delta r_R^L$ is relatively small. Consequently, the period of L-wiggles is comparable to the period of H-wiggles but certain phase shift is present.

3.9 Dependence on the density profile

The dependence of the probabilities on characteristics of density profile of the star (the initial density n_0 (see Fig. 3) and gradient of density change in the envelope) is shown in Fig. 5 for profiles A and B.

Let us first consider dependence of probabilities on k . With decrease of k the adiabaticity determined by $\lambda_n = r_R/k$ becomes stronger. Indeed, for fixed energy the resonance layer has larger radius r_R as k decreases. Consequently P_H becomes smaller and

- the 1-3 dip (in $\nu_e \rightarrow \nu_e$ channel) becomes deeper and reaches the adiabatic minimum, $P_{min} = s_{13}^2$, even for small values of 1-3 mixing (see Fig. 5, upper panel);
- adiabaticity is broken at higher energies ($E > 170$ GeV for $\sin^2 2\theta_{13} = 0.08$), and correspondingly, the wiggles (which are manifestations of the adiabaticity breaking) shift to higher energies;
- the amplitude of L-wiggles does not change significantly;
- period of wiggles decreases. This follows immediately from Eq. (3.34): r_R is larger and therefore the phase for a given E increases.

Similar features are present for $\nu_\mu \rightarrow \nu_\beta$ modes (see Fig. 5, lower panel). With decrease of k the adiabaticity both in H- and L- resonances improves. This means that in the range $E \gtrsim E_R^H$ the probabilities reach their adiabatic values. The amplitude of wiggles becomes smaller and period is substantially smaller. The latter is due to increase of r_R^L as in the case of H-wiggles.

For antineutrinos, decreases of gradient leads to stronger matter effect in the range ($10^2 - 10^4$) GeV, essentially extending region of the adiabatic conversion in the L-resonance to higher energies.

Effect of the inner density increase is illustrated in Fig. 3. There are two consequences of this increase: (i) shift of the resonance energies and therefore whole energy region of

matter effects to smaller energies; (ii) improvement of adiabaticity in both resonances due to the fact that for a given energy the radii of resonance layers increase. This, in turn, leads to the following observational consequences:

- the dip due to 1-3 resonance shifts to smaller energies and starts at $E = 60 - 80$ GeV for the factor of 2 density increase;
- the dip (peak) reaches the adiabatic minimum (maximum) for the survival (transition) channels; e.g. for $P(\nu_e \rightarrow \nu_e) \approx \sin^2 \theta_{13}$ and $P(\nu_\mu \rightarrow \nu_e) \approx 0.5(1 - \sin^2 \theta_{13})$;
- the H-wiggles have smaller period and so there are more wiggles on the nonadiabatic edge;
- the L-wiggles have smaller amplitude at low energy which then increases with energy. This is related to good adiabaticity in the L-channel and small P_L which increase with energy. Period of wiggles becomes smaller.
- Due to better adiabaticity the asymptotics are achieved at higher energies.

The antineutrino probabilities are affected very weakly and mainly in the range $(10^2 - 10^3)$ GeV.

On the contrary, with decrease of the initial density in the envelope and increase of the gradient, the matter-affected region shrinks: the region shifts to higher energies but its non-adiabatic edge - to lower energies.

4. Properties of conversion probabilities

Let us consider dependence of conversion probabilities in specific channels on neutrino parameters θ_{13} , θ_{23} as well as on the type of mass hierarchy.

4.1 Probabilities of $\nu_e \rightarrow \nu_\beta$ transitions

In Fig. 4.1 we show the $\nu_e \rightarrow \nu_\beta$, $\beta = e, \mu, \tau$ probabilities as functions of neutrino energy for different values of the 1-3 mixing angle. Properties of these probabilities can be well understood using the considerations in the previous sections.

1. In asymptotics according to (3.13) we have the averaged 3ν - oscillation probability in vacuum:

$$P(\nu_e \rightarrow \nu_e) = \sum_i |U_{ei}|^4 = \cos^4 \theta_{13} \left(1 - \frac{1}{2} \sin^2 2\theta_{12} \right) + \sin^4 \theta_{13}. \quad (4.1)$$

For $\nu_e \rightarrow \nu_\mu$ channel the probability equals $P(\nu_e \rightarrow \nu_\mu) = \sum_i |U_{ei}|^2 |U_{\mu i}|^2$, etc.

2. In the range $E_R^L \ll E \ll E_R^H$, inserting the matrix of probabilities (3.19) into Eq. (3.10) we obtain

$$P(\nu_e \rightarrow \nu_e) = |U_{e2}|^2(1 - |U_{e3}|^2) + |U_{e3}|^4 = |U_{e2}|^2 - |U_{e3}|^2(|U_{e2}|^2 - |U_{e3}|^2), \quad (4.2)$$

or in terms of the angles: $P(\nu_e \rightarrow \nu_e) = \cos^4 \theta_{13} \sin^2 \theta_{12} + \sin^4 \theta_{13}$. For the $\nu_e \rightarrow \nu_\mu$ channel we have

$$P(\nu_e \rightarrow \nu_\mu) = |U_{\mu 2}|^2(1 - |U_{e3}|^2) + |U_{\mu 3}|^2 |U_{e3}|^2 = |U_{\mu 2}|^2 + |U_{e3}|^2(|U_{\mu 3}|^2 - |U_{\mu 2}|^2), \quad (4.3)$$

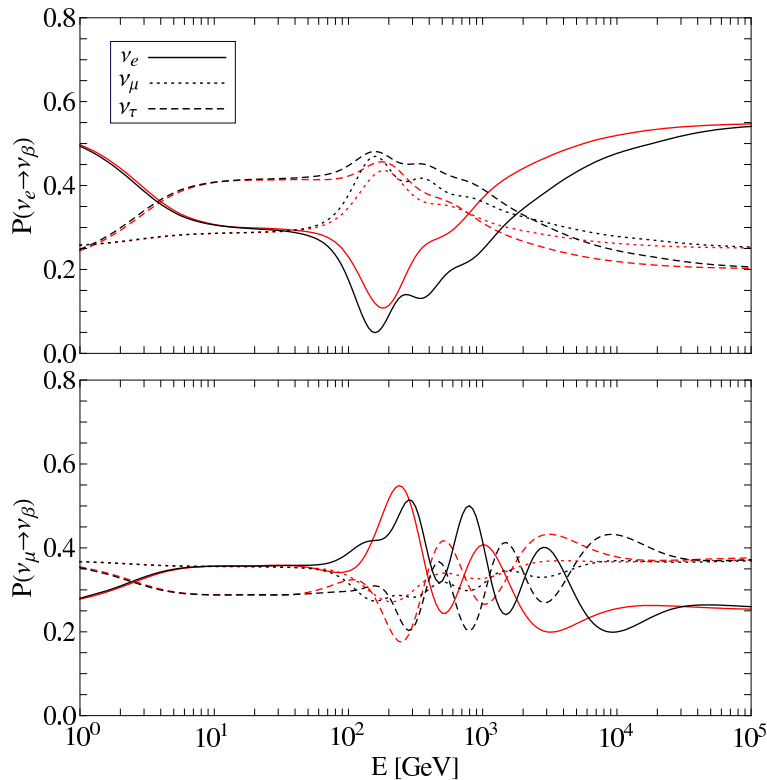


Figure 5: The $\nu_e \rightarrow \nu_\beta$ (top panel) and $\nu_\mu \rightarrow \nu_\beta$ (bottom panel) transition probabilities as functions of the neutrino energy for two different stellar density profiles, $\rho \propto r^{-3}$ (red curves) and $\rho \propto r^{-17/7}$ (black curves), but for the same initial density at R_0 . We used $\sin^2 2\theta_{13} = 0.08$, $\delta_{cp} = 0$ and normal mass hierarchy.

and similar expression for $P(\nu_e \rightarrow \nu_\tau)$ with substitution $|U_{\mu i}|^2 \rightarrow |U_{\tau i}|^2$.

3. For $E > E_R^H$ and large enough 1-3 mixing the adiabatic evolution gives according to (3.20) and (3.10)

$$P(\nu_e \rightarrow \nu_e) = |U_{e3}|^2, \quad P(\nu_e \rightarrow \nu_\mu) = |U_{\mu 3}|^2, \quad P(\nu_e \rightarrow \nu_\tau) = |U_{\tau 3}|^2. \quad (4.4)$$

These results reproduce the probabilities at $E \sim 200$ GeV for the 1-3 mixing $\sin^2 2\theta_{13} > 0.1$. For smaller 1-3 mixings the adiabaticity is broken already at $E \sim E_R^H$ and therefore $P(\nu_e \rightarrow \nu_e) > |U_{e3}|^2$.

If neutrinos are produced not too far (in energy scale) from the H-resonance, the ν_e -state contains non-negligible admixture of the ν_{2m} eigenstate:

$$\nu_e = \cos \theta_{13}^0 \nu_{2m} + \sin \theta_{13}^0 \nu_{3m}. \quad (4.5)$$

Adiabatic evolution of this combination will give then

$$P_*(\nu_e \rightarrow \nu_1) = 0, \quad P_*(\nu_e \rightarrow \nu_2) = \cos^2 \theta_{13}^0, \quad P_*(\nu_e \rightarrow \nu_3) = \sin^2 \theta_{13}^0,$$

and instead of (4.4) for $\nu_e \rightarrow \nu_e$ probability we obtain

$$P(\nu_e \rightarrow \nu_e) = \cos^2 \theta_{13}^0 \cos^2 \theta_{13} \sin^2 \theta_{12} + \sin^2 \theta_{13}^0 \sin^2 \theta_{13}.$$

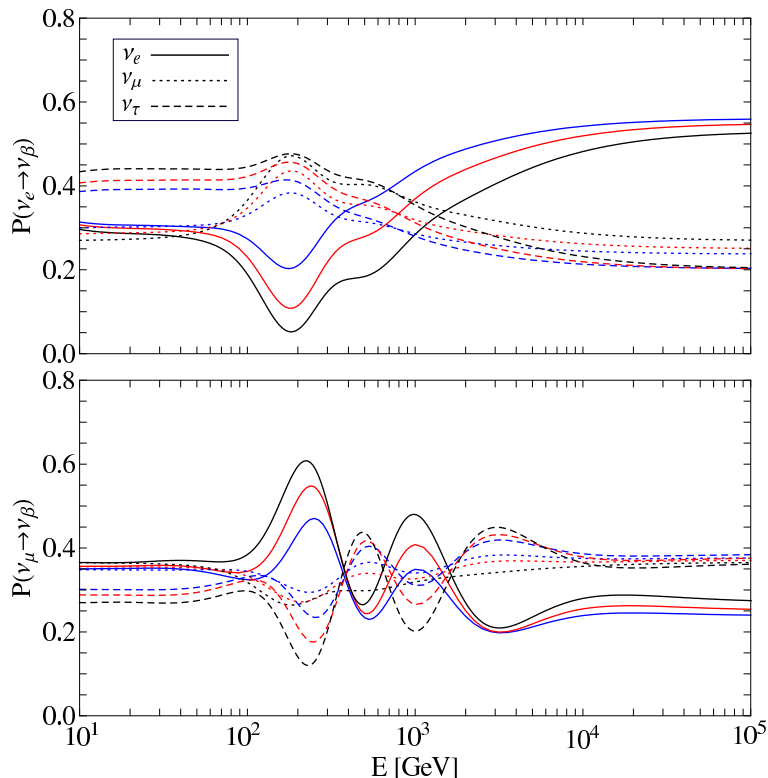


Figure 6: Probabilities for $\nu_e \rightarrow \nu_\beta$ (top panel) and $\nu_\mu \rightarrow \nu_\beta$ (bottom panel) transitions for different values of 1-3 mixing: $\sin^2 2\theta_{13} = 0.04$ (black lines), 0.08 (red) and 0.15 (blue lines). We take profile A, $\delta_{cp} = 0$, $\sin^2 \theta_{23} = 0.5$ and normal mass hierarchy.

For $E > E_R^H$ with increase of energy the adiabaticity violation becomes important.

The analytic results presented here allow one to understand the dependence of the probabilities on θ_{13} and θ_{23} . In asymptotics and in the intermediate region (plateau) the probabilities only weakly depend on θ_{13} (see Fig. 4.1): the corresponding corrections are proportional to $|U_{e3}|^2 = s_{13}^2$ (see (4.1), (4.2), (4.3)). The strongest effect is in the range of H-resonance and above it, where the 1-3 mixing is enhanced. For the dip in the adiabatic case we have $P \sim s_{13}^2$ (4.4). With decrease of s_{13}^2 the adiabaticity becomes broken and the survival probability increases. In the limit of very small s_{13}^2 the second dip disappears and we will have only one dip due to 1-2 mixing. The probabilities in other channels have an “inverted” dependence.

The dependence of probabilities on the 2-3 mixing is shown in Fig. 7. Note that the $\nu_e \rightarrow \nu_e$ probability does not depend on θ_{23} . The dependences of other probabilities have rather interesting feature: there are two energies $E_1 \approx 100$ GeV and $E_2 \approx 800$ GeV at which the probabilities do not depend on θ_{23} , and moreover, at $E_2 \approx 800$ GeV the probabilities in all the channels are equal. With increase of s_{23}^2 the $\nu_e \rightarrow \nu_\mu$ probability decreases at $E < E_1$ and $E > E_2$ and it increases in the interval $E_1 - E_2$. Indeed, according to (4.3) in the intermediate range $P(\nu_e \rightarrow \nu_\mu) = |U_{\mu 2}|^2 \approx c_{23}^2$, and in the 1-3 dip (4.4): $P(\nu_e \rightarrow \nu_\mu) = |U_{\mu 3}|^2 \approx s_{23}^2$. In asymptotics, a weaker change can be immediately

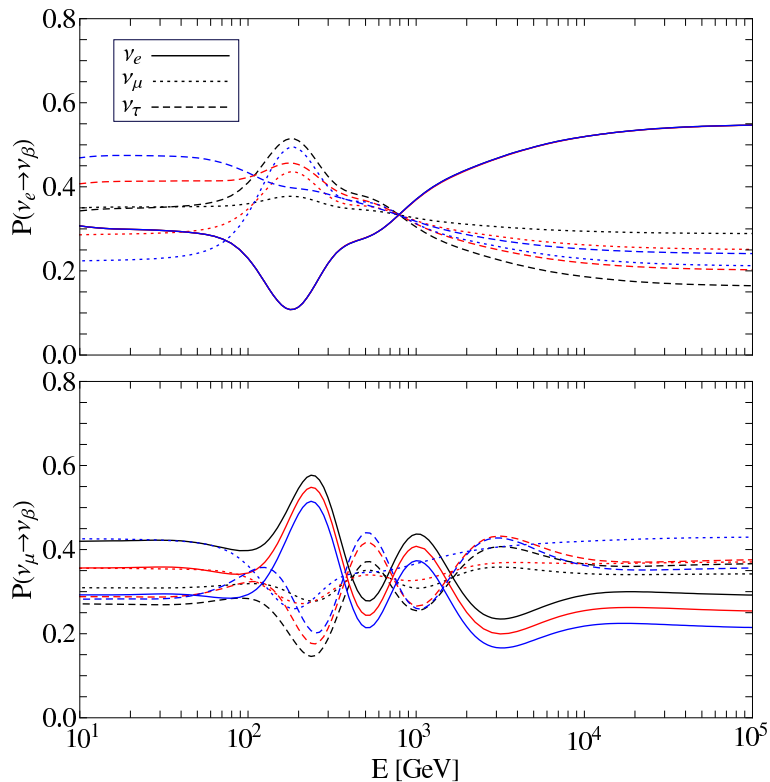


Figure 7: The $\nu_e \rightarrow \nu_\beta$ (top panel) and $\nu_\mu \rightarrow \nu_\beta$ (bottom panel) probabilities as functions of energy for different values of 2-3 mixing: $\sin^2 \theta_{23} = 0.4$ (black curves), 0.5 (red curves) and 0.6 (blue curves). We used profile A, $\sin^2 2\theta_{13} = 0.08$, $\delta_{CP} = 0$ and normal mass hierarchy.

understood from expression $P(\nu_e \rightarrow \nu_\mu) \approx |U_{e1}|^2|U_{\mu1}|^2 + |U_{e2}|^2|U_{\mu2}|^2$. The strongest dependence is in the plateau. The dependence for $\nu_e \rightarrow \nu_\tau$ channel is just inverted.

4.2 Probabilities of $\nu_\mu \rightarrow \nu_\beta$ and $\nu_\tau \rightarrow \nu_\beta$ transitions

The probabilities $P(\nu_\mu \rightarrow \nu_\beta)$ as functions of neutrino energy for different channels and two different values of 1-3 mixing are shown in Fig. 4.1. The main difference from the ν_e - channels is that ν_μ is not the eigenstate of the propagation basis (in contrast to ν_e) but combination of these states. This leads to more complicated expressions for the probabilities and additional interference effects. The probabilities equal

$$P(\nu_\mu \rightarrow \nu_\beta) = \sum_i P_*(\nu_\mu \rightarrow \nu_i)|U_{\beta i}|^2,$$

and explicit expressions for probabilities in different energy regions are given below.

The asymptotic values of probabilities for $E \ll E_L$ and $E \gg E_L$ equal

$$P(\nu_\mu \rightarrow \nu_\beta) = \sum_i |U_{\mu i}|^2 |U_{\beta i}|^2. \quad (4.6)$$

In the plateau we obtain from (3.10) and (3.19)

$$P(\nu_\mu \rightarrow \nu_\beta) = c_{23}^2 |U_{\beta 1}|^2 + s_{23}^2 |U_{e3}|^2 |U_{\beta 2}|^2 + s_{23}^2 c_{13}^3 |U_{\beta 3}|^2,$$

or

$$P(\nu_\mu \rightarrow \nu_\beta) = \frac{|U_{\tau 3}|^2 |U_{\beta 1}|^2}{1 - |U_{e 3}|^2} + \frac{|U_{\mu 3}|^2 |U_{e 3}|^2 |U_{\beta 2}|^2}{1 - |U_{e 3}|^2} + |U_{\beta 3}|^2 |U_{\mu 3}|^2, \quad (4.7)$$

where we used that

$$\sin^2 \theta_{23} \equiv \frac{|U_{\mu 3}|^2}{1 - |U_{e 3}|^2}, \quad \cos^2 \theta_{23} \equiv \frac{|U_{\tau 3}|^2}{1 - |U_{e 3}|^2}. \quad (4.8)$$

Above the H-resonance for large 1-3 mixing, which satisfies the adiabaticity condition, we find from (3.10) and (3.20)

$$\begin{aligned} P(\nu_\mu \rightarrow \nu_\beta) &= |U_{\beta 1}|^2 c_{23}^2 + |U_{\beta 2}|^2 s_{23}^2 \\ &= \frac{1}{1 - |U_{e 3}|^2} (|U_{\beta 2}|^2 |U_{\mu 3}|^2 + |U_{\beta 1}|^2 |U_{\tau 3}|^2). \end{aligned} \quad (4.9)$$

It reproduces in the first approximation correct values of the probabilities in the dip at $E \sim (150 - 170)$ GeV for large 1-3 mixing and for small gradients. Certain deviation of numerical results from analytic ones is a manifestation of the adiabaticity violation. For maximal 2-3 mixing we obtain from (4.9): $P(\nu_\mu \rightarrow \nu_\beta) = 0.5(1 - |U_{\beta 3}|^2)$.

As in the case of $\nu_e \rightarrow \nu_\beta$ the change of 1-3 mixing mainly affects the probabilities in the energy range above the H-resonance. With decrease of θ_{13} the jump probability increases and according to (3.40) the amplitude of wiggles, $I_\mu \propto \sqrt{1 - P_H}$, decreases.

The ν_τ - amplitudes and probabilities (they appear at the border of envelope due to oscillations inside jets) can be found from the ν_μ - amplitudes obtained in the previous subsection by substitutions: $U_{\mu 3} \rightarrow U_{\tau 3}$, $\sin \theta_{23} \rightarrow \cos \theta_{23}$, $\cos \theta_{23} \rightarrow -\sin \theta_{23}$.

4.3 Probabilities in antineutrino channels

There is no resonances in antineutrino channel for normal mass hierarchy and the dependence of the probabilities on energy is simpler (see Fig. 8). The 1-3 mixing is not enhanced and the conversion effects are mainly due to large 1-2 mixing at low energies (where this mixing is not suppressed).

The asymptotic values of the probabilities are the same as in the neutrino channels (4.6). There is no CP-violation asymmetries. In the intermediate region ($E_R^L < E < E_R^H$) we obtain from (3.10) and (3.22)

$$\begin{aligned} P(\bar{\nu}_e \rightarrow \bar{\nu}_\beta) &= |U_{\beta 1}|^2 (1 - |U_{e 3}|^2) + |U_{\beta 3}|^2 |U_{e 3}|^2 = |U_{\beta 1}|^2 - |U_{e 3}|^2 (|U_{\beta 1}|^2 - |U_{\beta 3}|^2), \\ P(\bar{\nu}_\mu \rightarrow \bar{\nu}_\beta) &= \frac{1}{1 - |U_{e 3}|^2} (|U_{\tau 3}|^2 |U_{\beta 2}|^2 + |U_{\mu 3}|^2 |U_{e 3}|^2 |U_{\beta 1}|^2) + |U_{\mu 3}|^2 |U_{\beta 3}|^2, \end{aligned} \quad (4.10)$$

($\beta = e, \mu, \tau$). They reproduce well the result of numerical computations in the range (10 – 50) GeV (see Fig. 8).

In the range $E \gtrsim E_R^H$, (150-180) GeV, the 1-3 mixing is suppressed by matter, so that $c_{13}^0 \approx 1$, $s_{13}^0 \approx 0$ in (3.22), and the flavor transition probabilities in the adiabatic approximation are

$$\begin{aligned} P(\bar{\nu}_e \rightarrow \bar{\nu}_\beta) &= |U_{\beta 1}|^2, \\ P(\bar{\nu}_\mu \rightarrow \bar{\nu}_\beta) &= \frac{1}{1 - |U_{e 3}|^2} (|U_{\tau 3}|^2 |U_{\beta 2}|^2 + |U_{\mu 3}|^2 |U_{\beta 3}|^2). \end{aligned} \quad (4.11)$$

Comparing the first probability with the one in (4.10) we conclude that $P(\bar{\nu}_e \rightarrow \bar{\nu}_e)$ only slightly increases in comparison with the intermediate region. With further increase of energy the probability decreases due to the adiabaticity violation, approaching the vacuum oscillation result. Correspondingly, $P(\bar{\nu}_e \rightarrow \bar{\nu}_\tau)$ is “inverted”.

The probabilities in antineutrino channels (in contrast to the neutrino resonance case) rather weakly depend on energy. Their dependence on the 1-3 mixing is weak (Fig. 8): according to (4.10), the corrections to $P(\bar{\nu}_e \rightarrow \bar{\nu}_\beta)$ are of the order $|U_{e3}|^2$, and corrections to $P(\bar{\nu}_\mu \rightarrow \bar{\nu}_\beta)$ are even smaller. The probabilities differ from their asymptotic values mainly in the intermediate range. Interestingly, the probabilities with $\bar{\nu}_\mu$ in final state (at least for zero δ and maximal 2-3 mixing) are not affected by matter.

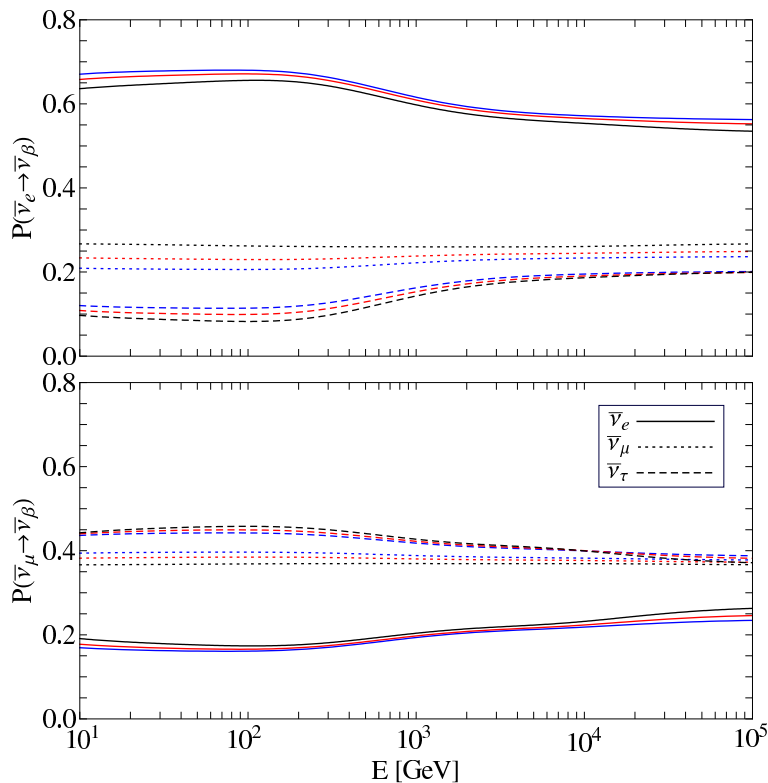


Figure 8: The same as in Fig. 4.1 for the antineutrino channels.

According to Fig. 9 the $\nu_e \rightarrow \nu_e$ probability does not depend on θ_{23} . Dependences of probabilities on 2-3 mixing are not very strong and well described by Eqs. (4.10) and (4.11).

4.4 Probabilities for the inverted mass hierarchy

Now the L-resonance is in the neutrino channels, whereas the H-resonance is in the antineutrino channels. Therefore the probabilities are given by some combinations of the results obtained for ν and $\bar{\nu}$ for the normal mass hierarchy (see Fig. 12). The differences appear when interplay of the two resonances (in the case of NH) becomes important.

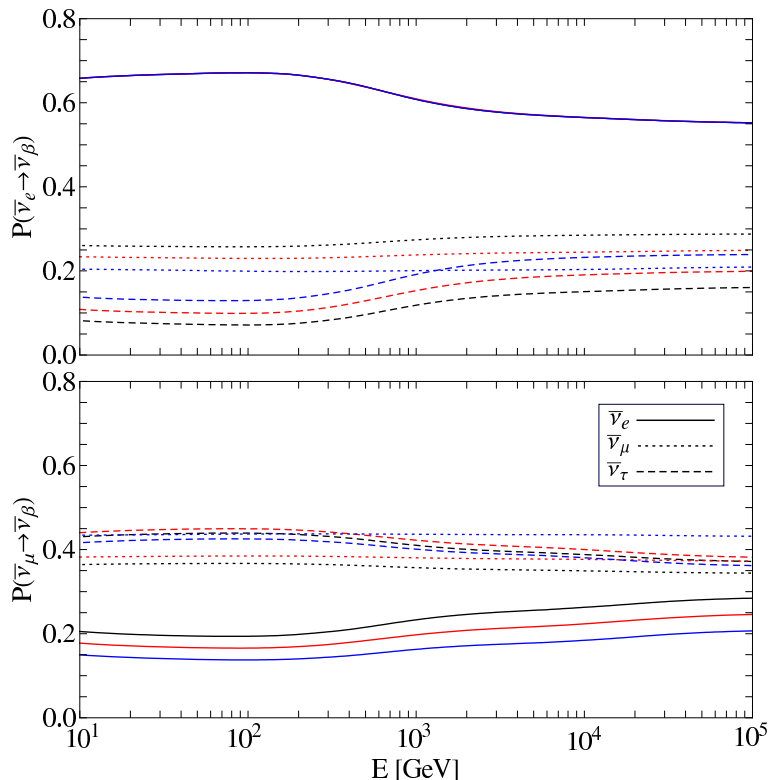


Figure 9: The same as in Fig. 7 for the antineutrino channels.

Let us consider first the neutrino probabilities. (i) The asymptotic values are the same as in the NH case. (ii) In the intermediate region we can use the same result as for NH (4.3) and (4.2). (iii) Above the H-resonance according to (3.20) and (3.10) we have

$$P(\nu_e \rightarrow \nu_\beta) = |U_{\beta 2}|^2, \quad (\beta = e, \mu, \tau), \quad (4.12)$$

which should be compared with the results in Eq. (4.4) for the normal mass hierarchy. In particular, $P(\nu_e \rightarrow \nu_e) = |U_{e2}|^2$. Comparing this result with (4.4) we see that the probability slightly increases in the H-resonance in contrast to the decrease in the NH case. According to Fig. 12 for $\sin^2 2\theta_{13} = 0.08$ the adiabaticity is broken already at $E = E_R^H$ and therefore values of probabilities deviate from those in Eq. (4.12).

In the intermediate energy region for the $(\nu_\mu \rightarrow \nu_\beta)$ channels we have the same results as in the case of normal mass hierarchy (4.7). Above the H-resonance, again the difference from the NH case appears since there is no level crossing. Using (3.23) we obtain flavor probabilities

$$\begin{aligned} P(\nu_\mu \rightarrow \nu_\beta) &= |U_{\beta 3}|^2 \sin^2 \theta_{23} + |U_{\beta 1}|^2 \cos^2 \theta_{23} \\ &= \frac{1}{1 - |U_{e3}|^2} (|U_{\beta 3}|^2 |U_{\mu 3}|^2 + |U_{\beta 1}|^2 |U_{\tau 3}|^2), \end{aligned}$$

which should be compared with Eq. (4.9).

Let us consider the antineutrino channels. In the intermediate energy range for the initial $\bar{\nu}_e$ we have the same results as in the NH case (4.10). Above the H-resonance (which

is now in the antineutrino channel) using Eq. (3.24) we obtain

$$\begin{aligned}
 P(\bar{\nu}_e \rightarrow \bar{\nu}_\beta) &= |U_{\beta 3}|^2, \\
 P(\bar{\nu}_\mu \rightarrow \bar{\nu}_\beta) &= \frac{1}{1 - |U_{e3}|^2} (|U_{\tau 3}|^2 |U_{\beta 2}|^2 + |U_{\mu 3}|^2 |U_{\beta 1}|^2).
 \end{aligned}
 \tag{4.13}$$

They reproduce correct values of the probabilities in the interval $E \sim (150 - 170)$ GeV.

4.5 Effects of oscillations inside jets

In Fig. 10 we compare the probabilities with and without oscillations in jet. As follows from these plots, the jet effect is very small and appears in the region above the H-resonance. This can be explained in the following way. Oscillations between neutrino production point inside jet and inner part of the envelope are described by $A_{jet}(\nu_\alpha \rightarrow \nu_\xi)$ introduced in Eq. (3.8). We assume that in the neutrino production region a jet has an average density $n_j \sim 1.5 \cdot 10^{20} \text{ cm}^{-3}$. The corresponding resonance energies equal: $E_{Rj}^L = 10^3 \text{ GeV}$ and $E_{Rj}^H = 6 \cdot 10^4 \text{ GeV}$ for the 1-2 and 1-3 mass splits correspondingly. Total matter width (column density) equals $n_j r_\nu \sim 9 \cdot 10^{29} \text{ cm}^{-2}$ which is much smaller than the refraction length [17] and therefore matter effect can be neglected. Indeed, for $E < E_R$ the potential is smaller than the kinetic (vacuum) term, whereas for $E > E_R$ the oscillation length is much smaller than the baseline, so that vacuum mimicking situation is realized [31]. In general, amplitude of vacuum oscillations in the flavor basis can be written as

$$A_{jet}(\nu'_\alpha \rightarrow \nu'_\xi) = \delta_{\alpha\xi} + U'_{\alpha 3} U'_{\xi 3}{}^* \left(e^{i2\phi_{31}} - 1 \right) + U'_{\alpha 2} U'_{\xi 2}{}^* \left(e^{i2\phi_{21}} - 1 \right),
 \tag{4.14}$$

where $\phi_{31} \equiv \pi x/l_{31}$ and $\phi_{21} \equiv \pi x/l_{21}$ are half oscillation phases inside jet. Vacuum oscillation lengths for the two modes equal $l_{13} = 10^{10} \text{ cm}$ ($E/100 \text{ GeV}$), and $l_{12} = 3 \cdot 10^{11} \text{ cm}$ ($E/100 \text{ GeV}$). The typical length of the neutrino trajectory inside jet $r_\nu \sim 6 \cdot 10^9 \text{ cm}$, and therefore for $E \gtrsim 60 \text{ GeV}$ the phase $\phi_{21} \approx 0$. So, we can neglect oscillations due to 1-2 mass split and consider non-averaged vacuum oscillations due to 1-3 mass splitting only. Then the amplitudes (4.14) become

$$A_{jet}(\nu'_\alpha \rightarrow \nu'_\xi) = \delta_{\alpha\xi} + U'_{\alpha 3} U'_{\xi 3}{}^* \eta(x),
 \tag{4.15}$$

where

$$\eta(x) \equiv \left[e^{i2\phi_{31}(x)} - 1 \right].
 \tag{4.16}$$

According to (3.4) the mixing matrix elements in the propagation basis are given by

$$U'_{\alpha 3} = \vec{U}_3 \equiv (s_{13}, 0, c_{13}), \quad \alpha = (e, \mu, \tau).$$

Thus, the S-matrix of transitions inside jet (4.15) can be written as

$$S_{jet} = I + \eta \vec{U}_3 \vec{U}_3^T = \begin{pmatrix} 1 + \eta s_{13}^2 & 0 & \eta s_{13} c_{13} \\ 0 & 1 & 0 \\ \eta s_{13} c_{13} & 0 & 1 + \eta c_{13}^2 \end{pmatrix}.$$

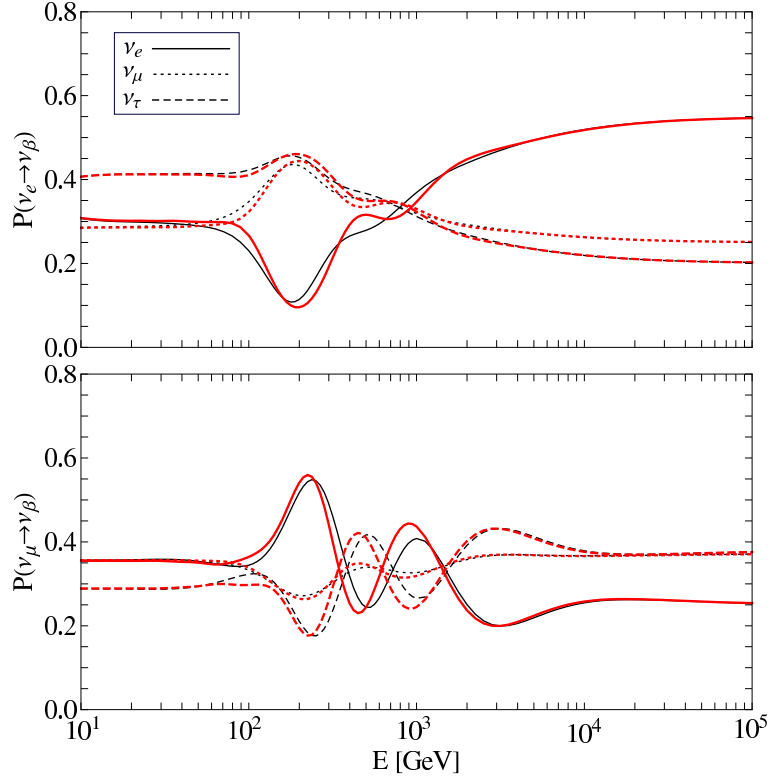


Figure 10: The $\nu_e \rightarrow \nu_\beta$ (top panel) and $\nu_\mu \rightarrow \nu_\beta$ (bottom panel) transition probabilities with oscillations in the jet (thick red curves) and without oscillations in jet (thin black curves). We used $\sin^2 2\theta_{13} = 0.08$, $\sin^2 \theta_{23} = 0.5$ and $\delta_{CP} = 0$ in normal mass hierarchy.

Inserting this matrix into (3.11) we obtain the total S-matrix inside the star:

$$S_* = \begin{pmatrix} 1 + \eta s_{23}^2 & 0 & \eta s_{13} c_{13} \\ \eta s_{13} c_{13} s_{23} e^{i\delta} & c_{23} & s_{23} e^{i\delta} (1 + \eta c_{23}^2) \\ \eta s_{13} c_{13} c_{23} e^{i\delta} & -s_{23} & c_{23} e^{i\delta} (1 + \eta c_{23}^2) \end{pmatrix} \times S_{env}, \quad (4.17)$$

where $(S_{env})_{\alpha i} \equiv A_{env}(\nu'_\alpha \rightarrow \nu_i)$.

In the adiabatic approximation the S-matrix in the envelope equals the mixing matrix at the inner part of the envelope: $S_{env} = U_m^0$ and the latter is given in Eq. (3.16). Inserting this matrix into (4.17) we obtain explicitly

$$S_* = \begin{pmatrix} 0 & c_{13}^0 (1 + \eta s_{23}^2) - \eta s_{13}^0 s_{13} c_{13} & s_{13}^0 (1 + \eta s_{23}^2) + \eta c_{13}^0 s_{13} c_{13} \\ -c_{23} & \eta c_{13}^0 s_{13} c_{13} s_{23} e^{i\delta} - s_{13}^0 s_{23} e^{i\delta} (1 + \eta c_{23}^2) & \eta s_{13}^0 s_{13} c_{13} s_{23} e^{i\delta} + c_{13}^0 s_{23} e^{i\delta} (1 + \eta c_{23}^2) \\ -s_{23} & \eta c_{13}^0 s_{13} c_{13} c_{23} e^{i\delta} - s_{13}^0 c_{23} e^{i\delta} (1 + \eta c_{23}^2) & \eta s_{13}^0 s_{13} c_{13} c_{23} e^{i\delta} + c_{13}^0 c_{23} e^{i\delta} (1 + \eta c_{23}^2) \end{pmatrix}. \quad (4.18)$$

Consider this matrix in specific energy ranges. In the intermediate energy range ($c_{13}^0 = c_{13}$, $s_{13}^0 = s_{13}$) it is

$$S_* = \begin{pmatrix} 0 & c_{13} & s_{13}(1 + \eta) \\ -c_{23} & -s_{13} s_{23} e^{i\delta} & c_{13} s_{23} e^{i\delta} (1 + \eta) \\ -s_{23} & -s_{13} c_{23} e^{i\delta} & c_{13} c_{23} e^{i\delta} (1 + \eta) \end{pmatrix}.$$

Corrections due to oscillation inside jet are given by the terms $\propto \eta$. Since $(1 + \eta) = e^{i2\phi_{13}}$ and $|(1 + \eta)|^2 = 1$, no corrections to the probabilities appear due to oscillations in jet. An absence of the corrections is related to the particular initial state (mixing in matter) in the envelope, the adiabatic evolution in the envelope and loss of coherence on the way from the star to the Earth.

Above the H-resonance ($c_{13}^0 \approx 0$, $s_{13}^0 \approx 1$) we have in the adiabatic approximation

$$S_* = \begin{pmatrix} 0 & -\eta s_{13} c_{13} & 1 + \eta s_{13}^2 \\ -c_{23} & -s_{23} e^{i\delta} (1 + \eta c_{13}^2) & \eta s_{13} c_{13} s_{23} e^{i\delta} \\ -s_{23} & -c_{23} e^{i\delta} (1 + \eta c_{13}^2) & \eta s_{13} c_{13} c_{23} e^{i\delta} \end{pmatrix}. \quad (4.19)$$

The probabilities are given by moduli squared of the S_* elements: $P_*(\nu_\alpha \rightarrow \nu_i) \equiv |(S_*)_{\alpha i}|^2$. Then, according to (4.19) corrections appear. Note that $|1 + \eta c_{13}^2|^2 = |1 + \eta^* s_{13}^2|^2$. Explicitly we obtain from (4.19) the probabilities for ν_e -channels:

$$P_*(\nu_e \rightarrow \nu_1) = 0, \quad P_*(\nu_e \rightarrow \nu_2) = s_{13}^2 c_{13}^2 |\eta|^2, \quad P_*(\nu_e \rightarrow \nu_3) = |1 + s_{13}^2 \eta|^2. \quad (4.20)$$

Now corrections are non-zero but they are suppressed by small factor s_{13}^2 .

For the ν_μ -channels we obtain from (4.19)

$$P_*(\nu_\mu \rightarrow \nu_1) = c_{23}^2, \quad P_*(\nu_\mu \rightarrow \nu_2) = s_{23}^2 |1 + c_{13}^2 \eta|^2, \quad P_*(\nu_\mu \rightarrow \nu_3) = s_{23}^2 s_{13}^2 c_{13}^2 |\eta|^2, \quad (4.21)$$

and again the corrections are small, being suppressed by s_{13}^2 .

From expression for S_* it follows that in the adiabatic case the probabilities do not depend on δ : the S_* -matrix elements either do not depend on δ or are proportional to the overall phase factor $e^{i\delta}$.

Similarly, for antineutrinos the probabilities of transitions are not affected by oscillations inside jet in the intermediate range. Above the H-resonance, according to (4.19),

$$P_*(\bar{\nu}_e \rightarrow \bar{\nu}_1) = |1 + s_{13}^2 \eta|^2, \quad P_*(\bar{\nu}_e \rightarrow \bar{\nu}_2) = 0, \quad P_*(\bar{\nu}_e \rightarrow \bar{\nu}_3) = s_{13}^2 c_{13}^2 |\eta|^2.$$

$$P_*(\bar{\nu}_\mu \rightarrow \bar{\nu}_1) = s_{13}^2 c_{13}^2 s_{23}^2 |\eta|^2, \quad P_*(\bar{\nu}_\mu \rightarrow \bar{\nu}_2) = c_{23}^2, \quad P_*(\bar{\nu}_\mu \rightarrow \bar{\nu}_3) = s_{23}^2 |1 + c_{13}^2 \eta|^2,$$

(compare with the corresponding results for neutrinos). As for the neutrino case, here we have non-zero corrections which are suppressed by small factor s_{13}^2 .

In the case of inverted mass hierarchy the amplitudes of oscillation inside jet are the same as for normal mass hierarchy, at least in our approximation (2ν -vacuum oscillations). So, the amplitudes A_{jet} equal the amplitudes in Eq. (4.15). Consequently, general formulas for the total amplitudes inside a star are given in Eq. (4.17).

For intermediate energy range we have exactly the same results as in the case of NH: there is no corrections due to oscillations inside jet. The difference appears at energies above H-resonance since now the level crossing and mixing in initial state are changed (see Fig. 2). We obtain the following expressions for probabilities:

$$P_*(\nu_e \rightarrow \nu_1) = 0, \quad P_*(\nu_e \rightarrow \nu_2) = |1 + s_{13}^2 \eta|^2, \quad P_*(\nu_e \rightarrow \nu_3) = s_{13}^2 c_{13}^2 |\eta|^2, \\ P_*(\nu_\mu \rightarrow \nu_1) = c_{23}^2, \quad P_*(\nu_\mu \rightarrow \nu_2) = s_{23}^2 s_{13}^2 c_{13}^2 |\eta|^2, \quad P_*(\nu_\mu \rightarrow \nu_3) = s_{23}^2 |1 + c_{13}^2 \eta|^2.$$

Note that probabilities of transitions to ν_1 are the same as in NH case, whereas the probabilities for transitions to ν_2 and ν_3 have been interchanged. The conclusion is the same as for NH: corrections are non-zero but they are suppressed by small factor s_{13}^2 . In the antineutrino channels in the intermediate energy range results are the same as in the case of NH. Above the H-resonance all the probabilities coincide with those we had obtained in Eqs. (4.20) and (4.21) for neutrinos.

An overall conclusion is that there is no corrections due to oscillations inside jets in the energy range between resonances and small corrections appear above the H-resonance. In general, the jet effect appears if the adiabaticity is broken.

4.6 CP-violation effects

Let us consider dependence of the oscillation probabilities on the CP-violation phase (see Figs. 11 and 12). Outside the matter affected energy interval, $E = (1 - 10^5)$ GeV, the probabilities equal the averaged oscillation probabilities in vacuum. Important feature is that the coherence of the mass states is lost after evolution inside star. Effects of the $(\nu_\alpha \rightarrow \nu_i)$ transitions sum up incoherently. So, projection back to final flavor state depends on moduli $|U_{\beta i}|^2$ and no interference effects appear. These probabilities depend on moduli squared of the mixing matrix elements and the interference terms are absent. In this case no CP-odd effects appear, the CP- as well as T-asymmetries vanish and $P(\nu_\alpha \rightarrow \nu_\beta) = P(\bar{\nu}_\alpha \rightarrow \bar{\nu}_\beta)$. The dependence on CP-violation phase originates from $|U_{\alpha i}|^2$ ($\alpha = \mu, \tau$, and $i = 1, 2$) and is rather weak since the terms with δ are proportional to $\sin \theta_{13}$.

The interference and CP-violation can be related to projection of the initial state onto the propagation basis states. To describe this let us first neglect oscillations inside jet and consider specific conversion channels.

1. $\nu_e \rightarrow \nu_\beta$ channels: since ν_e is the component of the propagation basis, no CP-violation appears in the projection and further conversions. $P(\nu_e \rightarrow \nu_e)$ does not depend on δ (see Figs. 11 and 12 top panels). $P(\nu_e \rightarrow \nu_\beta)$ ($\beta = \mu, \tau$) do depend on δ via $|U_{\beta i}|^2$ ($i = 1, 2$) (see Eq. (3.27)) via projection of the mass states onto the flavor state in the detector. Furthermore, for maximal 2-3 mixing with change of δ the $(\nu_e \rightarrow \nu_\mu)$ probability is transformed into $(\nu_e \rightarrow \nu_\tau)$ and *vice versa*, when δ increases from 0 to π , and at $\delta = \pi/2$

$$P(\nu_e \rightarrow \nu_\mu) = P(\nu_e \rightarrow \nu_\tau).$$

2. $\nu_\mu \rightarrow \nu_\beta$ channels: now according to (3.3)

$$\nu_\mu = c_{23}\nu'_\mu + s_{23}e^{i\delta}\nu'_\tau, \quad (4.22)$$

and the transition $\nu_\mu \rightarrow \nu_i$ has two channels via ν'_μ and ν'_τ which can interfere. So, as follows from (4.22) the probability equals

$$P_*(\nu_\mu \rightarrow \nu_i) = \left| c_{23}A_*(\nu'_\mu \rightarrow \nu_i) + s_{23}e^{i\delta}A_*(\nu'_\tau \rightarrow \nu_i) \right|^2. \quad (4.23)$$

The interference term depends on δ . As we saw before in the adiabatic case $A_*(\nu'_\mu \rightarrow \nu_i) = \delta_{i1}$ and $A_*(\nu'_\tau \rightarrow \nu_i) = (0, -s_{13}^0, c_{13}^0)$ (see Eq. (3.16)).

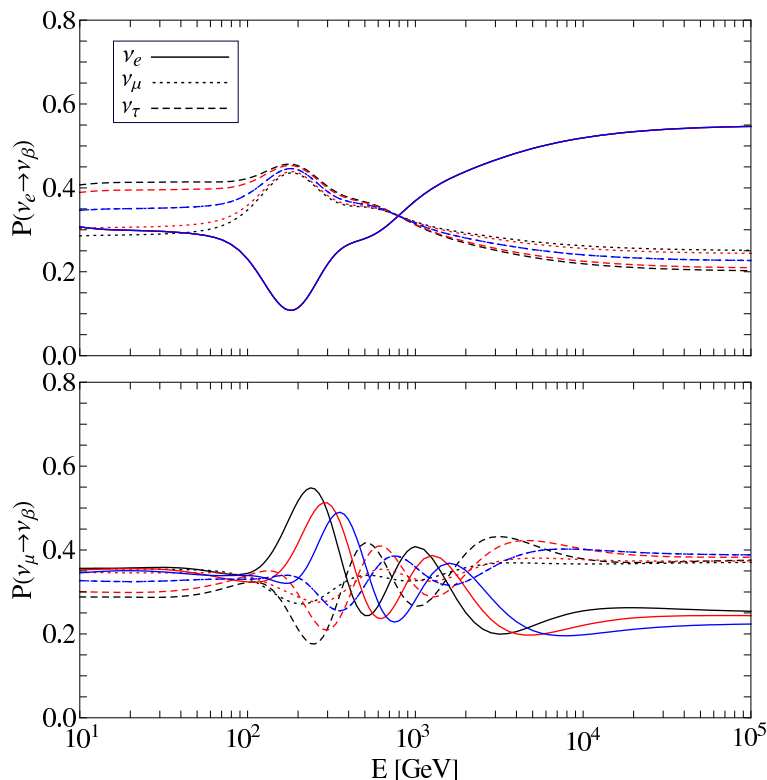


Figure 11: The probabilities as functions of energies for different values of the CP-phase $\delta_{cp} = 0$ (black curves), $\pi/4$ (red curves), and $\pi/2$ (blue curves). We take normal mass hierarchy and $\sin^2 2\theta_{13} = 0.08$.

Let us consider the interference in various energy ranges. In the intermediate energy range, according to (3.16) $\nu'_\mu \approx -\nu_{1m}$ and $\nu'_\tau \approx -s_{13}\nu_{2m} + c_{13}\nu_{3m}$. Since in this range ν_{1m} evolves adiabatically to ν_1 and the latter is orthogonal to the rest of the state, no interference appear between ν'_μ - and ν'_τ - channels in (4.23), and consequently,

$$P_*(\nu_\mu \rightarrow \nu_i) = |c_{23}A_*(\nu'_\mu \rightarrow \nu_i)|^2 + |s_{23}A_*(\nu'_\tau \rightarrow \nu_i)|^2.$$

This is in accordance with results (3.18). So, the interference and dependence on δ require adiabaticity violation, which is realized above the H-resonance. For $E \gtrsim E_R^H$ we have $s_{13}^0 \approx 1$, $\nu'_\mu \approx -\nu_{1m}$, and $\nu'_\tau \approx -\nu_{2m}$. Therefore

$$P_*(\nu_\mu \rightarrow \nu_i) = \left| c_{23}A_*(\nu_{1m} \rightarrow \nu_i) + s_{23}e^{i\delta}A_*(\nu_{2m} \rightarrow \nu_i) \right|^2,$$

and due to adiabaticity violation, both amplitudes in this equation are non zero simultaneously for $i = 1$ and 2 . The phase δ appears in the interference term in combination with the oscillation phase and therefore with change of δ the wiggles above the H-resonance shift (see Fig. 11). It might be practically impossible to disentangle the effect of δ from ϕ_L . Similar consideration holds for ν_τ .

Thus, in adiabatic energy range the dependence of the flavor probabilities on δ follows from the projection of mass states onto the flavor states in the detector only. The projection

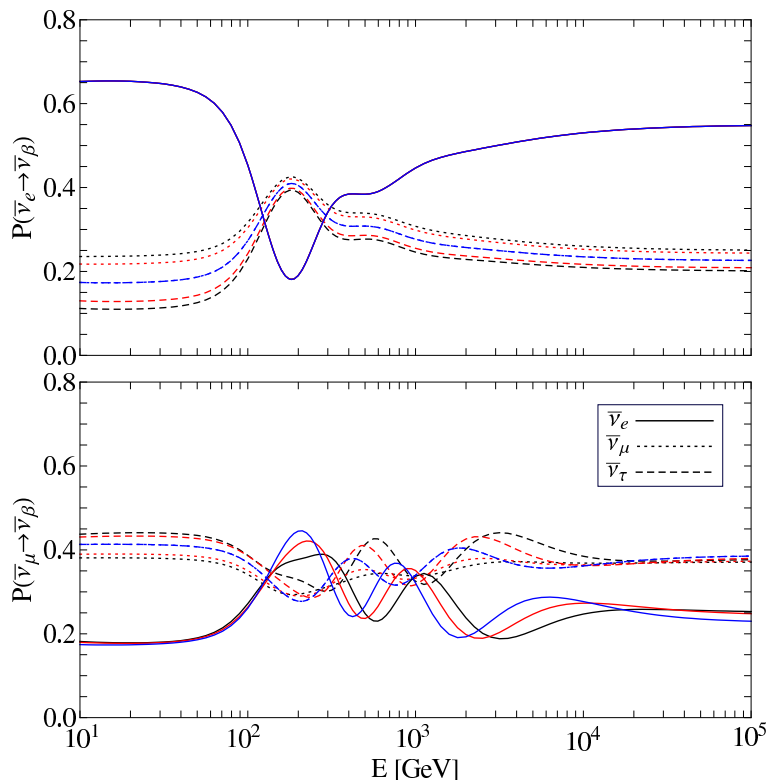


Figure 12: The same as in Fig. 11 for antineutrinos and the case of inverted mass hierarchy.

of the original flavor state onto the eigenstate of propagation gives an additional dependence on δ only if the adiabaticity is broken inside the star. In this connection let us take into account oscillations inside jets. From Eq. (4.17) we have

$$A_*(\nu_e \rightarrow \nu_i) = A_{env}(\nu_e \rightarrow \nu_i) + \eta s_{13} [s_{13} A_{env}(\nu_e \rightarrow \nu_i) + c_{13} A_{env}(\nu'_\tau \rightarrow \nu_i)], \quad (4.24)$$

where the second term is the jet effect. No dependence on the CP-phase appears here. For the $\nu_\mu \rightarrow \nu_i$ transitions, according to (4.17),

$$A_*(\nu_\mu \rightarrow \nu_i) = c_{23} A_{env}(\nu'_\mu \rightarrow \nu_i) + s_{23} e^{i\delta} A_{env}(\nu'_\tau \rightarrow \nu_i) + s_{23} c_{13} e^{i\delta} \eta [s_{13} A_{env}(\nu_e \rightarrow \nu_i) + c_{13} A_{env}(\nu'_\tau \rightarrow \nu_i)], \quad (4.25)$$

where the same combination of the amplitudes as in (4.24) enters the correction term. For $\eta = 0$ (no oscillations inside jet) this expression is reduced to the one in Eq. (4.23). The dependence on the CP-phase here is explicit. All other factors and amplitudes do not depend on δ .

Let us consider the antineutrino channels. General form of the amplitudes is the same as for neutrinos with the following changes: $\delta \rightarrow -\delta$, and $\theta_{ij}^m \rightarrow \bar{\theta}_{ij}^m$ which corresponds to change $V \rightarrow -V$. The amplitudes of oscillations inside jet are unchanged; they are essentially the 2ν -oscillations in vacuum in our approach.

5. Fluxes at the Earth

5.1 Flavor ratios

We compute the fluxes at the Earth separately for neutrinos and antineutrinos keeping in mind that in future experiments the signs of charged leptons may, in principle, be determined. The fluxes at the Earth equal:

$$\Phi_{\nu_\alpha} = \Phi_{\nu_\mu}^0 P(\nu_\mu \rightarrow \nu_\alpha) + \Phi_{\nu_e}^0 P(\nu_e \rightarrow \nu_\alpha) = \Phi_{\nu_\mu}^0 [P(\nu_\mu \rightarrow \nu_\alpha) + \epsilon P(\nu_e \rightarrow \nu_\alpha)],$$

where $\alpha = e, \mu, \tau$, and ϵ is given by Eq. (2.8). Similar expressions will be used for antineutrinos with substitution $\epsilon \rightarrow \bar{\epsilon}$. Let us introduce the flavor ratios as

$$r_{\alpha/\mu} \equiv \frac{\Phi_{\nu_\alpha}}{\Phi_{\nu_\mu}} = \frac{P(\nu_\mu \rightarrow \nu_\alpha) + \epsilon P(\nu_e \rightarrow \nu_\alpha)}{P(\nu_\mu \rightarrow \nu_\mu) + \epsilon P(\nu_e \rightarrow \nu_\mu)},$$

and for antineutrinos

$$r_{\bar{\alpha}/\mu} \equiv \frac{\Phi_{\bar{\nu}_\alpha}}{\Phi_{\nu_\mu}} = \frac{\Phi_{\bar{\nu}_\mu}^0}{\Phi_{\nu_\mu}^0} \frac{P(\bar{\nu}_\mu \rightarrow \bar{\nu}_\alpha) + \bar{\epsilon} P(\bar{\nu}_e \rightarrow \bar{\nu}_\alpha)}{P(\nu_\mu \rightarrow \nu_\mu) + \epsilon P(\nu_e \rightarrow \nu_\mu)},$$

normalizing all the fluxes at the Earth to the ν_μ -flux at the Earth.

According to Fig. 1 the ratio of original fluxes decrease with energy as

$$\frac{\Phi_{\nu_\mu}^0}{\Phi_{\nu_\mu}^0} = \begin{cases} 1; & E \lesssim 10 \text{ GeV} \\ 0.5; & E \gtrsim 300 \text{ GeV}. \end{cases} \quad (5.1)$$

The ratios contain complete information relevant for observations. Properties of the flavor ratios can be easily understood from properties of probabilities. If the charge of lepton produced by a neutrino is not defined, and thus, the experiment sums up signals of neutrinos and antineutrinos, observables are determined by the ratio:

$$r_{(\alpha+\bar{\alpha})/\mu} \equiv \frac{\Phi_{\nu_\alpha} + \xi_\alpha \Phi_{\bar{\nu}_\alpha}}{\Phi_{\nu_\mu} + \xi_\mu \Phi_{\bar{\nu}_\mu}} = \frac{r_{\alpha/\mu} + \xi_\alpha r_{\bar{\alpha}/\mu}}{1 + \xi_\mu r_{\bar{\mu}/\mu}},$$

where ξ_α describe ratios of antineutrino and neutrino cross-sections and corresponding efficiencies of detection. Note that contribution of antineutrinos is suppressed by about 0.2 - 0.3 due to smaller cross-section ($\xi_\alpha \sim 1/2$) and smaller original flux (another factor 1/2).

At energies below 10^5 GeV, ν_e and ν_τ can not be distinguished: both produce the showering events. The double-bang events which are signatures of the ν_τ -interaction can be identified at much higher energies [34]. Thus, with existing detectors one can study the ratio of the showering and tracking events (with muon track in the final state) $r_{sh/tr}$. In the first approximation it is determined by the ratio of the sum of ν_e - and ν_τ - fluxes to the ν_μ - fluxes:

$$r_{sh/tr} = \frac{\Phi_{\nu_e} + \xi_e \Phi_{\bar{\nu}_e} + \Phi_{\nu_\tau} + \xi_\tau \Phi_{\bar{\nu}_\tau}}{\Phi_{\nu_\mu} + \xi_\mu \Phi_{\bar{\nu}_\mu}} = \frac{r_{e/\mu} + \xi_e r_{\bar{e}/\mu} + r_{\tau/\mu} + \xi_\tau r_{\bar{\tau}/\mu}}{1 + \xi_\mu r_{\bar{\mu}/\mu}}. \quad (5.2)$$

This expression should be corrected (even neglecting misidentification of events): (i) certain part of ν_τ -flux contributes via transitions: $\nu_\tau \rightarrow \tau \rightarrow \mu$ to the tracking events (see e.g. [35]);

(ii) neutral current interactions (not affected by oscillations) contribute to the showering events.

To a good approximation, for $E > 100$ GeV, the charged current cross-sections are equal for all three flavors and therefore we can sum up the ν_e and ν_τ fluxes at the detector. (Note that still one should subtract the channel $\nu_\tau \rightarrow \tau \rightarrow \mu$ which leads to the tracking event.) Therefore if the initial flux is composed of ν_μ , the total flux which produces showering events is determined by the probability

$$P_{sh} = \sum_i P_*(\nu_\mu \rightarrow \nu_i)(|U_{ei}|^2 + (1 - b_\mu)|U_{\tau i}|^2),$$

where $b_\mu \sim 0.2$ is the fraction of $\tau \rightarrow \mu$ decays. Using unitarity we find

$$P_{sh} \equiv \sum_i P_*(\nu_\mu \rightarrow \nu_i)(1 - |U_{\mu i}|^2) = 1 - \sum_i P_*(\nu_\mu \rightarrow \nu_i)|U_{\mu i}|^2 - b_\mu \sum_i P_*(\nu_\mu \rightarrow \nu_i)|U_{\tau i}|^2,$$

and the latter equals $P_{sh} = 1 - P_{tot}(\nu_\mu \rightarrow \nu_\mu) - b_\mu \sum_i P_*(\nu_\mu \rightarrow \nu_i)|U_{\tau i}|^2$. If ν_μ dominates in the initial state, $P_{tot}(\nu_\mu \rightarrow \nu_\mu)$ determines the probabilities of all observable events when $\tau \rightarrow \mu$ decays are neglected. In the presence of the original ν_e -flux we have

$$P_{sh} \equiv 1 - P(\nu_\mu \rightarrow \nu_\mu) + \epsilon[1 - P(\nu_e \rightarrow \nu_\mu)].$$

5.2 Properties of the flavor ratios

In Figs. 13 - 18 we show the flavor ratios $r_{\alpha/\mu}$ and $r_{\bar{\alpha}/\mu}$ ($\alpha = e, \mu, \tau$) as functions of neutrino energies, values of neutrino parameters and density profiles. For illustration we use two extreme original flavor contents: (i) $\epsilon : 1 : 0$, where $\epsilon = \epsilon(E)$ and according to Fig. 1 it decreases from 0.5 at $E \lesssim 10$ GeV down to 10^{-2} at high energies. This content would correspond to strong suppression of muon decays in medium of jet without secondary acceleration. (ii) $1 : 2 : 0$ which corresponds to $\epsilon = 0.5$ and does not depend on energy. This could be realized when additional acceleration of secondary muons occurs in jets.

Consider first $\epsilon : 1 : 0$. For very small ϵ we have

$$r_{\alpha/\mu} \approx \frac{\Phi_{\nu_\alpha}}{\Phi_{\nu_\mu}} \approx \frac{P(\nu_\mu \rightarrow \nu_\alpha)}{P(\nu_\mu \rightarrow \nu_\mu)}.$$

Furthermore, since $P(\nu_\mu \rightarrow \nu_\mu)$ has weak dependence on energy, the ratio essentially repeats behavior of $P(\nu_\mu \rightarrow \nu_\alpha)$. According to Fig. 13 (upper panel), and in agreement with our analytic considerations, the ratio $r_{e/\mu}$ has an asymptotic value ~ 0.7 and the deviation of this value from the flavor equilibration is due to the original flavor content. In the intermediate region (plateau), due to equality $P(\nu_\mu \rightarrow \nu_e) \approx P(\nu_\mu \rightarrow \nu_\mu)$ for maximal 2-3 mixing we have $r_{e/\mu} \approx 1$. The 1-3 peak (at $E = 200$ GeV) is slightly enhanced in comparison to the peak in probability.

In the plateau for maximal 2-3 mixing we have $P(\nu_\mu \rightarrow \nu_\tau) < P(\nu_\mu \rightarrow \nu_\mu)$, and consequently, $r_{\tau/\mu} \sim 0.8$. The wiggles of $P(\nu_\mu \rightarrow \nu_\tau)$ and $r_{\tau/\mu}$ have an opposite phase as compared with wiggles of $P(\nu_\mu \rightarrow \nu_e)$ and $r_{e/\mu}$, and the amplitude of wiggles of showers/tracks ratio is suppressed. For maximal 2-3 mixing the asymptotic value equals $r_{\tau/\mu} \approx 1$. Due to

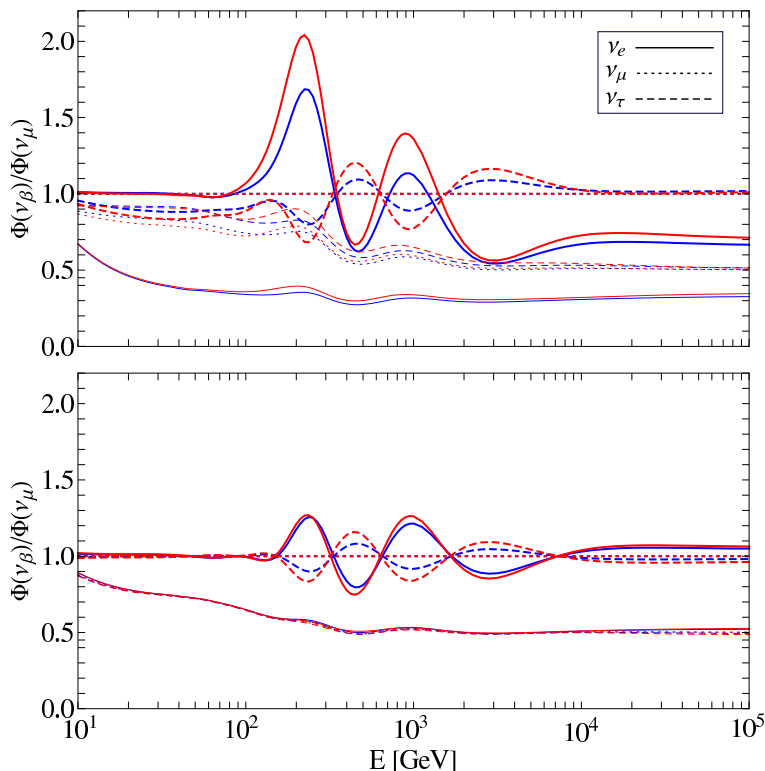


Figure 13: Neutrino and antineutrino flavor ratios (fluxes normalized to the ν_μ flux) as functions of the neutrino energy for two different values of 1-3 mixing, $\sin^2 2\theta_{13} = 0.04$ (blue lines) and 0.08 (red lines) and two different original flavor contents: $\epsilon : 1 : 0$ (upper panel) and $1 : 2 : 0$ (lower panel). The thick (thin) lines correspond to the neutrino (antineutrino) fluxes. We used profile A, $\sin^2 \theta_{23} = 0.5$, $\delta_{cp} = 0$ and normal mass hierarchy.

opposit phase the $r_{\tau/\mu}$ and $r_{e/\mu}$ wiggles compensate each other in the ratio $r_{sh/tr}$, leading to substantially smaller amplitude of $r_{sh/tr}$ wiggles (see Fig. 19).

For anineutrinos (see Fig. 13) the ratio

$$r_{\bar{\alpha}/\mu} \approx \frac{\Phi_{\bar{\nu}_\mu}^0}{\Phi_{\nu_\mu}^0} \cdot \frac{P(\bar{\nu}_\mu \rightarrow \bar{\nu}_\alpha)}{P(\nu_\mu \rightarrow \nu_\mu)}$$

follows to a large extent the ratio of original fluxes in (5.1) in the case of NH. An additional distortion due to oscillations is rather small. In particular, difference of high and low energy asymptotics in flavor ratios is related to difference of ratio $\Phi_{\bar{\nu}_\mu}^0/\Phi_{\nu_\mu}^0$ at high and low energies.

For the original flavor content $(1 : 2 : 0)$ (bottom panels) the ν_e -flux and its transformations substantially change the flavor ratios at the Earth. In the intermediate range, still $r_{e/\mu} \approx 1$ as a consequence of the equality $P(\nu_e \rightarrow \nu_e) \approx P(\nu_e \rightarrow \nu_\mu)$ for maximal 2-3 mixing. At and above the energy of H-resonance the probability $P(\nu_e \rightarrow \nu_e)$ has a dip, whereas $P(\nu_e \rightarrow \nu_\mu)$ has a peak and above the peak/dip they have wiggles of the opposit sign. Therefore the wiggles of ratio $r_{e/\mu}$ are strongly attenuated. This ratio deviates from 1 (equilibration) which is the signature of the matter effect only in the region $(10^2 - 10^4)$ GeV and maximal effect is about 30%. Similarly, for the ratio $r_{\tau/\mu}$ substantial attenuation

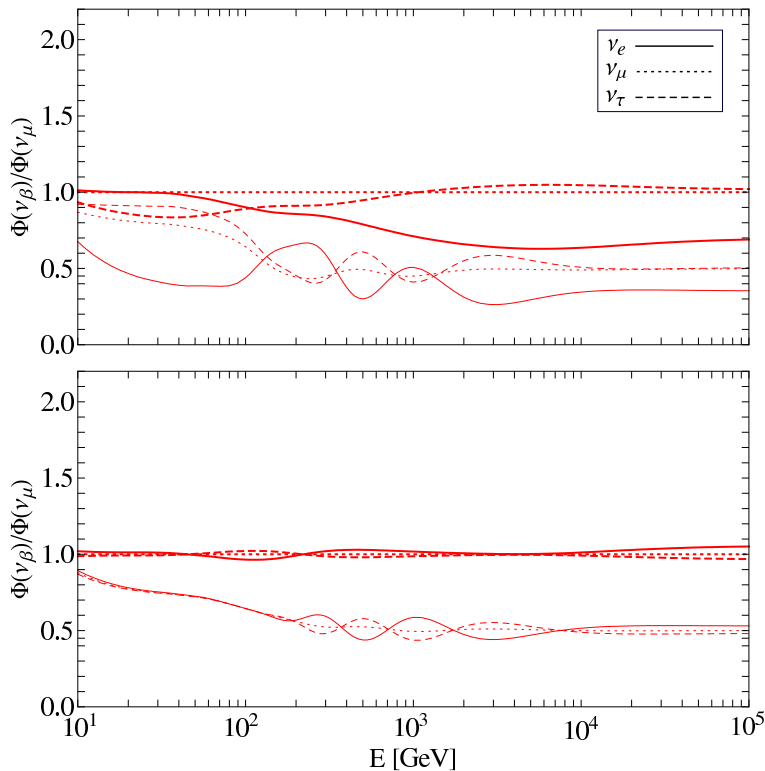


Figure 14: The same as in Fig. 13 for inverted mass hierarchy and only for $\sin^2 2\theta_{13} = 0.08$.

occurs. Moreover, the wiggles of $r_{e/\mu}$ and $r_{\tau/\mu}$ have opposite phase, and therefore the wiggles in the $r_{sh/tr}$ are further suppressed (see Fig. 19).

As follows from Fig. 13, the highest sensitivity to θ_{13} is in the range of H-resonance peak and wiggles: $E = (10^2 - 10^3)$ GeV. (Recall that in the ν_μ -channels the peak is also due to resonance enhancement of the 1-3 mixing.) With decrease of θ_{13} adiabaticity is broken stronger and the amplitude of wiggles becomes smaller.

Let us consider the case of inverted mass hierarchy (see Fig. 14). For the $(\epsilon : 1 : 0)$ original content, as in the case of NH the asymptotics is $r_{e/\mu} \approx 0.7$ and in the plateau $r_{e/\mu} \approx 1$. In the H-resonance region there is no peak, the ratio decreases with increase of energy from 1 to the asymptotic value. This dependence is modulated by small wiggles. The peak appears in the H-resonance region in the antineutrino ratio $r_{\bar{e}/\mu}$.

For the original flavor ratio $(1 : 2 : 0)$, due to strong compensations of contributions from different channels the matter effect on the flavor ratios is small.

Let us consider dependence of the flavor ratios on other neutrino parameters.

1. The phase of wiggles changes with δ : wiggles shift (see Fig. 15). Changes in plateau as well as in the asymptotics are rather weak.
2. Dependence of flavor ratios, as functions of energy, on the 2-3 mixing is strong (see Fig. 16). The strongest dependence is for $r_{e/\mu}$ (NH) in the plateau region: as we already mentioned, for maximal 2-3 mixing the probabilities of $(\nu_\mu \rightarrow \nu_e)$ and $(\nu_\mu \rightarrow \nu_\mu)$ transitions coincide. However with change of θ_{23} they change in the opposite way: one increases and

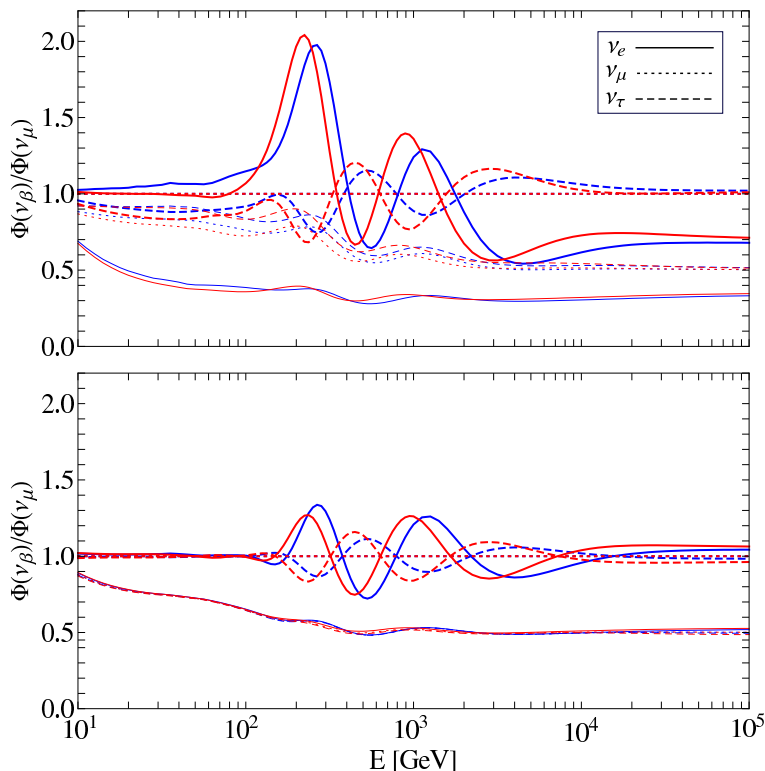


Figure 15: Neutrino and antineutrino flavor ratios as functions of the neutrino energy for two different values of the CP phase δ : 0 (red lines) and $\pi/4$ (blue lines) and two different original flavor contents: $\epsilon : 1 : 0$ (upper panel) and $1 : 2 : 0$ (lower panel). The thick (thin) lines correspond to the neutrino (antineutrino) fluxes. We used profile A, $\sin^2 \theta_{23} = 0.5$, $\sin^2 \theta_{13} = 0.08$ and normal mass hierarchy.

another decreases, as can be seen in Fig. 16. The $\nu_\mu \rightarrow \nu_\tau$ probability changes much weaker. Note that asymptotic values also vary rather substantially, whereas the change in the 1-3 peak is small. Thus, determination of $r_{e/\mu}$ in the plateau region would be the most sensitive to search for deviation of the 2-3 mixing from maximal. For the original flavor content $(1 : 2 : 0)$ the dependence on θ_{23} is weaker.

Consider dependence of the flavor ratios on the density profile. With decrease of density gradient, k , (see Fig. 17) the evolution becomes more adiabatic, the 1-3 peak shifts to smaller energies and becomes wider; the amplitude of wiggles decreases, the region of wiggles extends to higher energies.

For the original flavor content $(1 : 2 : 0)$, there is substantial cancellation of contributions from the $\nu_\mu \rightarrow \nu_e$ and $\nu_e \rightarrow \nu_e$ transitions, since the transition and the survival probabilities have opposite dependence on energy.

Dependence of the ratios on the initial density n_0 is strong (see Fig. 18): with increase of n_0 the resonance peak shifts to lower energies, the period of wiggles decreases and number of wiggles increases; the amplitudes of wiggles become slightly smaller. In the case of $(1 : 2 : 0)$ original content, there is strong cancellation of contributions of $(\nu_\mu \rightarrow \nu_e)$ and $(\nu_e \rightarrow \nu_e)$ especially in the region of 1-3 peak. As a consequence, the region of wiggles

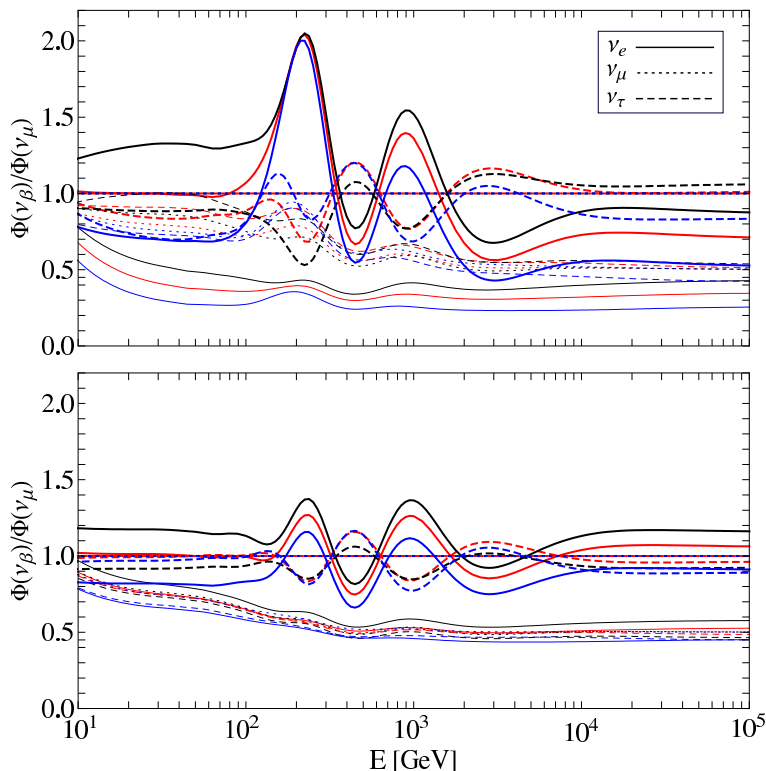


Figure 16: Neutrino and antineutrino flavor ratios as functions of the neutrino energy for different values of $\sin^2 \theta_{23}$: 0.4 (black lines), 0.5 (red lines), 0.6 (blue lines), and two different original flavor contents: $\epsilon : 1 : 0$ (upper panel) and $1 : 2 : 0$ (lower panel). The thick (thin) lines correspond to the neutrino (antineutrino) fluxes. We used profile A, $\sin^2 2\theta_{13} = 0.08$, $\delta_{cp} = 0$ and normal mass hierarchy.

starts from about 200 GeV.

In general, in the case of original ($\epsilon : 1 : 0$) content, dependences of the flavor ratios on the neutrino parameter as well as on parameters of the star are much stronger, and this makes hidden jets to be more prospective than the observable jets as far as investigation of neutrino parameters is concerned.

In Fig. 19 we show the ratio of shower-to-track events on the neutrino energy defined in Eq. (5.2). Qualitatively, this dependence repeats the corresponding dependence of the flavor ratio $r_{e/\mu}$ with L-wiggles and asymmetric asymptotics at high and low energies. However relative size of the wiggles, and in general, matter effects (deviations from the averaged oscillation result) is further suppressed. As we mentioned before, this suppression is due to contribution of the $\nu_\mu \rightarrow \nu_\tau$ transition, $r_{\tau/\mu}$, as well as the contributions of antineutrinos which have small matter effect for the normal mass hierarchy. According to Fig. 19, the structures in $r_{sh/tr}$ due to conversion in the matter of the star are up to 40 – 50%. This should be compared with factor of (2 - 2.5) effect in the ratio $r_{e/\mu}$. The effect is smaller for the inverted mass hierarchy. Substantial deviations from the averaged VO result are in the energy range ($10^2 - 2 \cdot 10^3$) GeV which can be extended to ($30 - 5 \cdot 10^3$) GeV for smaller density gradient or larger density in the inner part of the envelope (bottom

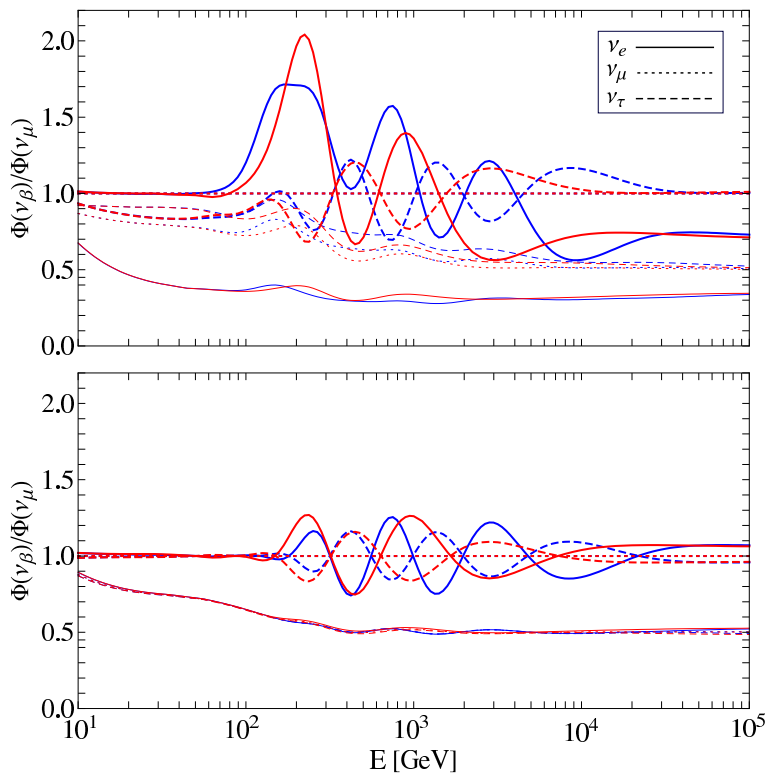


Figure 17: Neutrino and antineutrino flavor ratios as functions of the neutrino energy for different density profiles: A (red lines) B (blue lines) and two different original flavor contents: $\epsilon : 1 : 0$ (upper panel) and $1 : 2 : 0$ (lower panel). The thick (thin) lines correspond to the neutrino (antineutrino) fluxes. We used $\sin^2 2\theta_{13} = 0.08$, $\delta_{CP} = 0$ and normal mass hierarchy.

panel). The size of the matter effect is much smaller: about $\pm 5\%$ in the case of initial ratio flavor ratio ($1 : 2 : 0$).

6. Discussion and conclusion

Hidden jets realize unique set up (configuration and conditions) in which at one hand protons can be accelerated up to high energies and then produce high energy neutrinos, and at the other hand these neutrinos cross large enough column density of matter on the way from production region so that flavor conversion in the matter of the star is important. We present detailed and comprehensive study of flavor conversion of neutrinos from hidden sources (jets) - astrophysical sources invisible in non-thermal γ rays or X rays. Our results differ from the results of paper [16].

1. The conversion is affected by matter of a star and the Earth in the energy interval $\sim (1 - 10^5)$ GeV. In this range the probabilities and flavor ratios substantially deviate from probabilities and ratios given by the averaged vacuum oscillations. The borders of this interval are determined by the largest density in the envelope, $E_L = E_L(n_0)$, and gradient of density in the envelope $\sim R_\star \Delta m_{31}^2 / 4\pi$ rather than on R_\star , the radius of the stellar envelope. The interval expands for larger initial density and smaller gradient. For

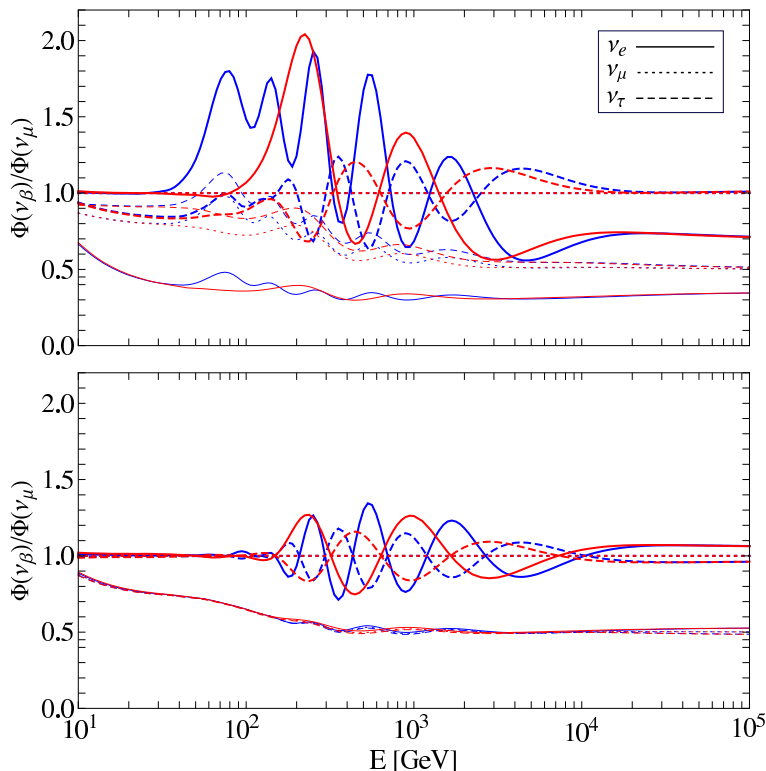


Figure 18: Neutrino and antineutrino flavor ratios as functions of the neutrino energy for the profile A with different inner number densities of electrons $n_0 = 10^{23} \text{ cm}^{-1}$ (red lines) and $n_0 = 2 \cdot 10^{23} \text{ cm}^{-1}$ (blue lines) and two different original flavor contents: $\epsilon : 1 : 0$ (upper panel) and $1 : 2 : 0$ (lower panel). The thick (thin) lines correspond to the neutrino (antineutrino) fluxes. We used $\sin^2 2\theta_{13} = 0.08$, $\delta_{cp} = 0$ and normal mass hierarchy.

energies below this interval matter effects can be neglected and with decrease of energy the probability converges to the averaged VO probability. Above the interval the adiabaticity is strongly broken and flavor evolution inside a star can be neglected. With increase of energy the probability converges to the averaged VO probability again.

2. We discussed in details physics involved in the production of neutrinos. Neutrinos are produced in π^- , μ^- and K^- -decays in strong magnetic fields which leads to very short wave packets of neutrinos. This, in turn, results in quick separation of the wave packets and loss of coherence, in spite of high neutrino energy. The coherence length is comparable with radius of star. The coherence is not restored in a detector due to finite energy resolution and large baselines. Therefore the overall evolution consists of the flavor-to-mass states transitions inside the star, loss of coherence, propagation of the nmmass staes in vacuum; so that incoherent fluxes of mass states arrive at the surface of the Earth. Detector projects these mass states back onto flavor states incoherently.

Inelastic scattering becomes important for high energies $\sim 10^4 \text{ GeV}$. To a good approximation this scattering is flavor invariant, and therefore factors out and does not influence the flavor conversion picture. It can be included in determination of the original neutrino spectra. We have estimated that some effect of $\nu - \nu$ scattering may show up at high

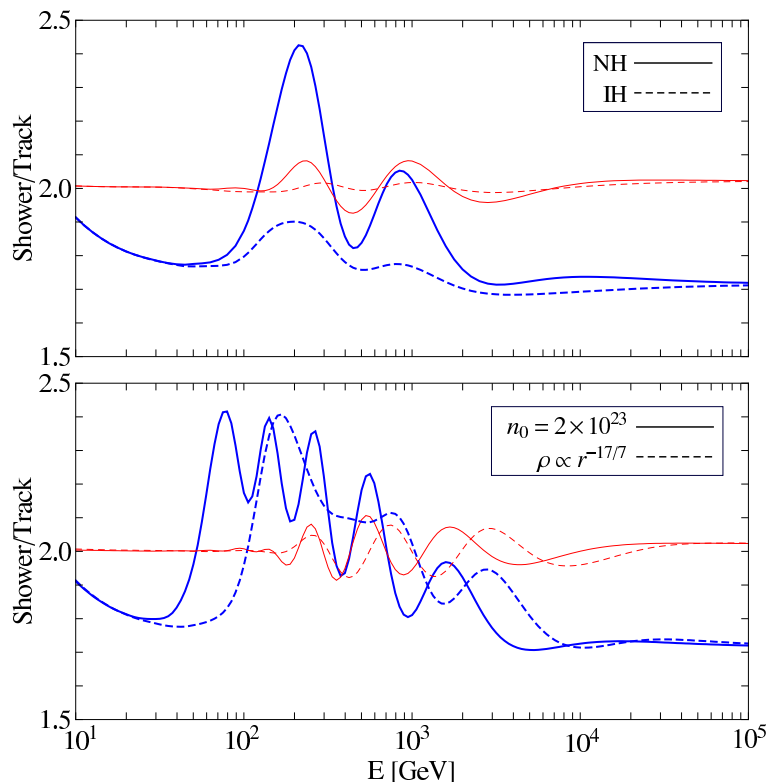


Figure 19: Ratio of the shower-to-track events as the functions of the neutrino energy for two different initial flavor content: $\epsilon : 1 : 0$ (blue lines) and $1:2:0$ (red lines) upper panel: for normal (solid) and inverted (dashed); we used profile A; lower panel: for $n_0 = 2 \times 10^{23} \text{ cm}^{-1}$ (solid lines) and for smaller gradient $k = 17/7$ (dashed lines). We used $\sin^2 2\theta_{13} = 0.08$, $\delta_{cp} = 0$.

energies where usual flavor conversion effect becomes small.

3. Mainly the neutrino flavor change is due to adiabatic and partially adiabatic conversion in the envelope of a star. Oscillations inside the Earth lead to an additional distortion of probabilities below 10 GeV. We show that probabilities as functions of neutrino energy have several generic features which are well controlled by the density profile crossed by neutrinos (initial density, density gradient). This includes

- Plateau in the intermediate energy range which is due to adiabatic conversion in the 1-2 resonance region. The Earth matter effect produces an oscillatory dip in the plateau at $E < 10 \text{ GeV}$.
- The dips or peaks (depending on channel) related to the 1-3 resonance at $E \gtrsim E_H$.
- Non-adiabatic edge of the energy profile is modulated by wiggles. The wiggles are new dynamical feature which is not realized in other objects. The wiggles are manifestations of interference induced by adiabaticity violation in the H-resonance (H-wiggles) and in L-resonance (L-wiggles).

Different features of the energy profile of the matter effect such as low energy border, plateau, the 1-3 peak/dip (its position and size), wiggles and asymptotics depend on

parameters of neutrino and star differently, so that one will be able to disentangle these dependences in principle. Position of these features depends on density profile of the star: in particular, on the density at the border between jet and envelope (n_0) and gradient of density in an envelope (k). The size of the matter effects depends on values of neutrino parameters as well as on original flavor content. In the adiabatic range there is no dependence on the profile (apart from lower border of the regions). Therefore plateau as well as the 1-3 peak (for large enough θ_{13} or small gradient) do not depend on a profile. Above the H-resonance in the adiabaticity violation range (the wiggles region) characteristics of probabilities depend both on profile and on neutrino parameters. In particular, number of wiggles is a measure of the density gradient in the envelope.

4. At the Earth one can, in principle, determine the flavor ratios $r_{e/\mu}$, $r_{\tau/\mu}$, $r_{\bar{e}/\mu}$, $r_{\bar{\tau}/\mu}$, $r_{\bar{\mu}/\mu}$ as functions of neutrino energy. To a large extent these ratios reproduce the energy dependence of probabilities. Independent measurements of these ratios would give very rich information on neutrino parameters, density profile of star and original flavor ratios which encode information about conditions inside jets. Effect of neutrino flavor conversion on these ratios is strong, modifying the ratios in certain energy ranges by factor 2 – 3. With present experimental techniques and detectors, however, one can determine the ratio of shower-to-track numbers of events only, without separation of neutrinos and antineutrinos. Sum of contributions from neutrinos and antineutrinos as well as from ν_e and ν_τ (which have an opposite phase) lead to significant damping of the observable conversion effect in $r_{sh/tr}$. The effect depends strongly on the original flavor content. It can reach 30 – 40 % for the content $\epsilon : 1 : 0$ ($\epsilon \ll 1$) and it is about 5 – 10% for $1 : 2 : 0$. In reality one can expect some intermediate situation.

5. Observability of the neutrino signal from hidden jets is beyond the scope of this paper, and here we just add some comments. There are two issues related to observability: (i) number of event in a given detector, and (ii) a possibility to identify signal and extract it from a background produced by the atmospheric neutrinos. These issues have been discussed partly in [16]. Detection of signal from individual source would require large detector and/or a source in a nearby galaxy such as M82 and NGC253. Signatures include high energy neutrino events from certain directions during ~ 10 sec. which can be repeated. There should be a correlation between the jetted neutrino signal ($E \gtrsim 1$ GeV) with burst of low energy thermal neutrinos ($E \sim 5 - 50$ MeV) generated during the core collapse. Thermal 10–50 MeV neutrinos are also produced in a jet since the shell density and temperature are initially very high at the base of the jet. No significant delay is expected between the thermal and high-energy neutrinos that are produced in the jet. There can be significant delay between the emission of core-collapse thermal neutrinos and jet thermal/high-energy neutrinos depending on whether the core collapses directly to a black hole or via an intermediate neutron star stage. The thermal neutrino emission from core-collapse preceding the high-energy (and more thermal) neutrino emission and the time-delay between the two can be used as a probe to learn about the core-collapse and jet formation processes.

In case of a successful supernova, with or without jet break out, optical lightcurve can be extrapolated back to the time of explosion and to check temporal correlation with any neutrino signal detected from the same direction in the sky. This can largely reduce the

atmospheric neutrino and muon background. A neutrino detector setup outside the Earth's atmosphere, e.g., in space or on the Moon, as the technology develops, can of course greatly improve the detection prospect of astrophysical neutrinos.

It is expected that parameters of jets change during jet duration which leads to time dependence of neutrino signals we have discussed. In principal, it opens unique possibility to monitor evolution of jets with neutrinos.

The neutrino oscillation signatures from hidden jets are modified in the case of isotropic diffuse flux. To identify this flux one can use distortion of the energy spectrum in the energy range where atmospheric neutrinos are not affected by oscillations. In general if the diffuse flux is dominated by hidden sources as discussed here, the measured flavor ratio will differ significantly from the usual (1 : 1 : 1) ratio expected from the optically thin sources in the GeV – TeV range.

Acknowledgements

We thank Cecilia Lunardini for helpful comments on the manuscript. SR would like to thank the Abdus Salam International Centre for Theoretical Physics for warm hospitality where part of this work was completed.

A. Meson and lepton energy losses

High energy π and K are subject to energy losses due to hadronic πp and $K p$ interactions with cross-sections $\sigma_{\pi p/K p} \approx (2/3)\sigma_{pp}$, and due to synchrotron radiation in the strong magnetic field before they decay. The cooling time scales due to these processes are

$$t'_{had}(E'_{\pi(K)}) \approx \frac{E'_{\pi(K)}}{n'_p \sigma_{\pi(K)p} \Delta E'_{\pi(K)}} \sim 10^{-5} \text{ s},$$

for hadronic interactions, where $\Delta E'_{\pi(K)} \approx 0.5 E'_{\pi(K)}$ is the average inelasticity and we ignored the logarithmic factor in cross-section, and

$$t'_{em}(E'_j) \approx \left(\frac{E'_j}{\text{GeV}} \right)^{-1} \left(\frac{B'}{10^9 \text{ G}} \right)^{-2} \times \begin{cases} 0.34 \text{ s}; & j = K \\ 2.2 \times 10^{-3} \text{ s}; & j = \pi \\ 7.0 \times 10^{-4} \text{ s}; & j = \mu \end{cases}$$

for the synchrotron cooling. As can be seen, from these equations, the meson energy losses are initially dominated by hadronic and later by electromagnetic process [8, 9]. With a decay time scale $t'_{j,dec} = \tau_j(E'_j/m_j)$, where τ_j is the mean lifetime, π and K decay without significant energy losses below $E'_{K,b1} \sim 400 \text{ GeV}$ and $E'_{\pi,b1} \sim 50 \text{ GeV}$ (which corresponds to $t'_{dec} \approx t'_{had}$). The electromagnetic losses become important at energies above $E'_{K,b2} \sim 35 \text{ TeV}$ and $E'_{\pi,b2} \sim 220 \text{ GeV}$ (which corresponds to $t'_{em} \approx t'_{had}$). Thus we can define a suppression factor to be multiplied with the production fluxes of π and K before they decay as

$$\zeta_j(E'_j) \approx \begin{cases} 1; & E'_j \lesssim E'_{j,b1} \\ t'_{j,had}/t'_{j,dec} \approx (E'_j/E'_{j,b1})^{-1}; & E'_{j,b1} \lesssim E'_j \lesssim E'_{j,b2} \\ t'_{j,em}/t'_{j,dec} \approx (E'_{j,b1}/E'_{j,b2})(E'_j/E'_{j,b2})^{-2}; & E'_j \gtrsim E'_{j,b2} \end{cases}$$

Note that muons from π - or K -decays are also subject to synchrotron energy losses which dominate above $E'_{\mu,b} \approx 6$ GeV and the μ -flux before decay will be suppressed by a factor $\sim (E'_{\mu}/E'_{\mu,b})^{-2}$. Thus, the ν 's from μ -decay channels contribute little to the total flux at high energy. Also, the contributions to the ν fluxes from πp - and $K p$ -interactions is small and we ignore those.

B. Comparison of the conversion formulas in Ref. [16] and in this paper

General formula (3.6) for the conversion probabilities differ from that used in the paper [16]. Consequently, results of this paper differ from the results in [16]. According to [16] the flavor probability equals

$$P(\nu_{\alpha} \rightarrow \nu_{\beta}) = \sum_{\gamma} P_{*}(\nu_{\alpha} \rightarrow \nu_{\gamma}) \bar{P}_V(\nu_{\gamma} \rightarrow \nu_{\beta}), \quad (\text{B.1})$$

where ν_{γ} is a flavor neutrino state, and $\bar{P}_V(\nu_{\gamma} \rightarrow \nu_{\beta})$ is the averaged oscillation probability in vacuum. Taking explicit expression for the latter we can rewrite the probability (B.1) as

$$P(\nu_{\alpha} \rightarrow \nu_{\beta}) = \sum_{\gamma} P_{*}(\nu_{\alpha} \rightarrow \nu_{\gamma}) \sum_i |U_{\beta i}|^2 |U_{\gamma i}|^2 \quad (\text{B.2})$$

or

$$P(\nu_{\alpha} \rightarrow \nu_{\beta}) = \sum_i |U_{\beta i}|^2 \sum_{\gamma} |A_{*}(\nu_{\alpha} \rightarrow \nu_{\gamma})|^2 |U_{\gamma i}|^2, \quad (\text{B.3})$$

where $A_{*}(\nu_{\alpha} \rightarrow \nu_{\gamma})$ is the amplitude of probability of the corresponding flavor transition. On the other hand, expression for the probability (3.6) we use in this paper can be rewritten as

$$P(\nu_{\alpha} \rightarrow \nu_{\beta}) = \sum_i |U_{\beta i}|^2 \left| \sum_{\gamma} A_{*}(\nu_{\alpha} \rightarrow \nu_{\gamma}) U_{\gamma i} \right|^2, \quad (\text{B.4})$$

which clearly differs from (B.3). The difference is that instead of the flavor states ν_{γ} at the exit from the star, we take the mass states ν_i which are the eigenstates of propagation in vacuum and these states lose coherence. In (B.3) the averaging was taken for oscillations outside the star, and oscillations of mass states are not averaged inside the star. Therefore Eq. (B.3) leads to fast oscillatory picture which corresponds to oscillations inside the envelope in the interval from $r_{jet} - R_{*}$. In our consideration the wiggles also appear. However they appear in the adiabaticity violation range only, i.e. above the H-resonance. There is no wiggles in the adiabatic part. Furthermore, the period of wiggles in the energy scale is much larger: the phase of wiggles is determined by the oscillation phase on the way from the production point to the H- resonance region (for H-wiggles) and to the L-resonance (for the L-wiggles) which is much smaller than total size of the envelope $r_{jet} - R_{*}$.

C. The Earth matter effect

The mass-to-flavor transition probabilities inside the Earth can be written as

$$P_E(\nu_i \rightarrow \nu_{\beta}) = |(U_{23} \Gamma_{\delta} S_E U')_{\beta i}|^2 = |(U_{23} \Gamma_{\delta} S_E U_{13} U_{12})_{\beta i}|^2, \quad (\text{C.1})$$

where according to (3.4) U' gives projection of the mass states onto the states of the propagation basis, S_E is the S-matrix for transitions inside the Earth in the propagation basis, and $U_{23}\Gamma_\delta$ projects the propagation basis onto the flavor basis. (If $S_E = I$, the probability (C.1) is reduced to $|(U_{PMNS})_{\beta i}|^2$.)

Let us find explicit expression for S_E for $E \gtrsim 1$ GeV where substantial neutrino flux from jets exists. For the Earth densities this energy range is far above the L-resonance and the 1-2 mixing is strongly suppressed. So, the problem is reduced to 2ν -oscillations due to the 1-3 mixing. For definiteness we will take normal mass hierarchy and consider for simplicity the evolution in the approximation of constant density. In this case

$$S_E = U'_m D U_m{}^\dagger, \quad (\text{C.2})$$

where

$$D = \text{diag}(e^{-i\phi_{12}}, 1, e^{-i\phi_{32}}). \quad (\text{C.3})$$

Here $\phi_{12} \equiv \phi_1 - \phi_2$, $\phi_{32} \equiv \phi_3 - \phi_2$, and $\phi_i = H_i t$ are the oscillation phases of the eigenstates in matter ν_{im} (H_i are the eigenvalues in matter). The mixing matrix in matter in the propagation basis, U'_m , for $E \gg E_L$ equals, according to (3.5),

$$U'_m \approx \begin{pmatrix} 0 & c_{13}^m & s_{13}^m \\ -1 & 0 & 0 \\ 0 & -s_{13}^m & c_{13}^m \end{pmatrix}.$$

Using this expression for U'_m and (C.3) we find from (C.2) the evolution matrix in the Earth:

$$S_E \approx \begin{pmatrix} A_{ee} & 0 & A_{e\tau} \\ 0 & -e^{-i\phi_{12}} & 0 \\ A_{e\tau} & 0 & A_{\tau\tau} \end{pmatrix}, \quad (\text{C.4})$$

where

$$A_{ee} = c_{13}^{m2} + s_{13}^{m2} e^{-i\phi_{32}}, \quad A_{e\tau} = s_{13}^m c_{13}^m (e^{-i\phi_{32}} - 1), \quad A_{\tau\tau} = s_{13}^{m2} + c_{13}^{m2} e^{-i\phi_{32}}. \quad (\text{C.5})$$

Inserting (C.4) into (C.1) we obtain the matrix of flavor-to-mass transition probabilities. In particular, we have

$$\begin{aligned} P(\nu_1 \rightarrow \nu_e) &= |c_{13}c_{12}A_{ee} - s_{13}c_{12}A_{e\tau}|^2, \\ P(\nu_2 \rightarrow \nu_e) &= |c_{13}s_{12}A_{ee} - s_{13}s_{12}A_{e\tau}|^2, \\ P(\nu_3 \rightarrow \nu_e) &= |s_{13}A_{ee} + c_{13}A_{e\tau}|^2. \end{aligned} \quad (\text{C.6})$$

Then for the flavor probability $\nu_e \rightarrow \nu_e$ with all transitions included we obtain using (3.9) and (3.19):

$$P(\nu_e \rightarrow \nu_e) = c_{13}^2 s_{12}^2 |c_{13}A_{ee} - s_{13}A_{e\tau}|^2 + s_{13}^2 |s_{13}A_{ee} + c_{13}A_{e\tau}|^2. \quad (\text{C.7})$$

This is reduced to the probability without oscillations inside the Earth (4.2) for $A_{ee} = 1$ and $A_{e\tau} = 0$. In the first approximation in s_{13} we have from (C.7)

$$P(\nu_e \rightarrow \nu_e) \approx s_{12}^2 |A_{ee}|^2 \approx s_{12}^2 \left(1 - \sin^2 2\theta_{13}^m \sin^2 \frac{\phi_{23}}{2} \right). \quad (\text{C.8})$$

According to this result the plateau is modulated by resonance oscillations: the oscillatory dip appears in the range $E \sim E_{13}^R \sim 6$ GeV. Typical width of the dip is given by $\Delta E \sim 2E_{13}^R \tan 2\theta_{13}$. So, for $\sin 2\theta_{13} = 0.08$ the modulations are in the range (4 – 8) GeV. Maximal depth depends on the zenith angle of the neutrino trajectory. The result (C.8) differs from the Earth matter effect on the solar neutrinos where both plateau and the Earth effect are due to 1-2 mixing and the Earth matter effect enhances the survival probability. Here the effect is opposite: the probability becomes smaller. The difference stems from the difference of density profile of the Sun and an envelope of a star. In particular, density in the central part of the Sun, where neutrinos are produced are much higher than maximal density in an envelope. As a result, in the case of jetted neutrinos, the Earth matter effect due to 1-2 mixing is at very low energies (< 0.2 GeV) - essentially in the low asymptotic region - below E_L . The Earth matter effect in the 1-2 mixing plateau is due to 1-3 mixing. This (to some extent) is similar to the 1-3 dip at $E \gtrsim 10^2$ GeV.

Detection of the Earth matter effect could give an information about neutrino properties and also about direction to the star. It is not clear though, if this effect can be ever extracted from the atmospheric neutrino background.

References

- [1] F. Halzen, arXiv:0910.0436v1 [astro-ph.HE]; V. Berezinsky, in Proc. 4th Int. Workshop “Neutrino Oscillations in Venice”, ed. Milla Baldo Ceolin, p. 137, arXiv:0901.1428 [astro-ph]; E. Waxman, *Science*, **315**, 63, (2007).
- [2] F. W. Stecker, C. Done, M. H. Salamon and P. Sommers, *Phys. Rev. Lett.* **66**, 2697 (1991); Erratum-ibid. **69**, 2738 (1992); L. Nellen, K. Mannheim and P. L. Biermann, *Phys. Rev. D* **47**, 5270 (1993); A. P. Szabo and R. J. Protheroe, *Astropart. Phys.* **2**, 375 (1994); A. Atoyan and C. D. Dermer, *Phys. Rev. Lett.* **87**, 221102 (2001); J. Alvarez-Muniz and P. Meszaros, *Phys. Rev. D* **70**, 123001 (2004).
- [3] E. Waxman and J. N. Bahcall, *Phys. Rev. Lett.* **78**, 2292 (1997); A. Atoyan and C. D. Dermer, *Phys. Rev. Lett.* **91** 071102 (2003); S. Razzaque, P. Meszaros and E. Waxman, *Phys. Rev. D* **69**, 023001 (2004); K. Murase, K. Ioka, S. Nagataki, T. Nakamura, *Astrophys. J.* **651**, L5 (2006); N. Gupta and B. Zhang, *Astropart. Phys.* **27**, 386 (2007).
- [4] E. Waxman and A. Loeb, *Phys. Rev. Lett.* **87**, 071101 (2001); X.-Y. Wang, S. Razzaque, P. Meszaros and Z.-G. Dai, *Phys. Rev. D* **76**, 083009 (2007).
- [5] J. Alvarez-Muniz and F. Halzen, *Astrophys. J.* **576**, L33 (2002); M. L. Costantini and F. Vissani, *Astropart. Phys.* **23**, 477 (2005).
- [6] S. Razzaque, P. Mészáros, and E. Waxman, *Phys. Rev. Lett.* **93**, 181101 (2004); **94**, 109903(E) (2005).
- [7] D. C. Leonard, A. V. Filippenko, A. J. Barth and T. Matheson, *Astrophys. J.* **536**, 239 (2000); L. Wang, D. A. Howell, P. Hoflich and J. C. Wheeler, *Astrophys. J.* **550**, 1030 (2001); J. Granot and E. Ramirez-Ruiz, *Astrophys. J.* **609**, L9 (2004).
- [8] S. Ando and J. F. Beacom, *Phys. Rev. Lett.* **95**, 061103 (2005).
- [9] S. Razzaque, P. Mészáros, and E. Waxman, *Mod. Phys. Lett. A*, **20**, 2351 (2005).

- [10] S. Ando, J. F. Beacom and H. Yuksel, *Phys. Rev. Lett.* **95**, 171101 (2005).
- [11] Fermi LAT Collaboration (A. A. Abdo, et al.), arXiv:0911.5327v1 [astro-ph.HE].
- [12] J. Ahrens et al. *Astropart. Phys.* **20**, 507 (2004).
- [13] ANTARES Collaboration (J. A. Aguilar et al.), *Astropart. Phys.* **26**, 314 (2006).
- [14] U. F. Katz, Presented at 2nd VLNT Workshop on Very Large Neutrino Telescope (VLNT2), Catania, Italy, 8-11 Nov 2005. Published in *Nucl. Instrum. Meth. A* **567**, 457 (2006).
- [15] M. Kowalski and A. Mohr, *Astropart. Phys.* **27**, 533 (2007).
- [16] O. Mena, I. Mocioiu and S. Razzaque, *Phys. Rev. D* **75**, 063003 (2007) [arXiv:astro-ph/0612325].
- [17] C. Lunardini and A. Y. Smirnov, *Nucl. Phys. B* **583**, 260 (2000) [arXiv:hep-ph/0002152].
- [18] Y. Farzan and A. Y. Smirnov, *Nucl. Phys. B* **805**, 356 (2008) [arXiv:0803.0495 [hep-ph]].
- [19] L. Wolfenstein, *Phys. Rev. D* **17** (1978) 2369; L. Wolfenstein, in “Neutrino-78”, Purdue Univ. C3, (1978); S. P. Mikheev and A. Y. Smirnov, *Sov. J. Nucl. Phys.* **42**, 913 (1985) [*Yad. Fiz.* **42**, 1441 (1985)]; S. P. Mikheev and A. Y. Smirnov, *Sov. Phys. JETP* **64**, 4 (1986) [*Zh. Eksp. Teor. Fiz.* **91**, 7 (1986)] [arXiv:0706.0454 [hep-ph]].
- [20] A. I. McFadyen and S. E. Woosley, *Astrophys. J.* **524**, 262 (1999).
- [21] A. A. Abdo, et al. [Fermi Collaboration], *Science*, **323**, 1688 (2009); A. A. Abdo, et al. [Fermi Collaboration & The Swift Team] *ApJL* (accepted), arXiv:0909.2470.
- [22] A. I. McFadyen, S. E. Woosley, and A. Heger, *Astrophys. J.* **550**, 410 (2001).
- [23] T. Piran, *Rev. Mod. Phys.* **76**, 1143 (2004); P. Meszaros, *Rept. Prog. Phys.* **69**, 2259 (2006).
- [24] T. K. Gaisser, “Cosmic Rays and Particle Physics”, Cambridge University Press (1990).
- [25] R. Enberg, M. H. Reno and I. Sarcevic, *Phys. Rev. D* **79**, 053006 (2009).
- [26] P. Lipari, *Astropart. Phys.* **1**, 195 (1993).
- [27] H. B. J. Koers and R. A. M. J. Wijers, arXiv:0711.4791v1
- [28] C. D. Matzner and C. F. McKee, *Astrophys. J.* **510**, 379 (1999).
- [29] B. Pontecorvo, *Zh. Eksp. Teor. Fiz.* **34** (1958) 247 [*Sov. Phys. JETP* **7** (1958) 172].
- [30] Z. Maki, M. Nakagawa and S. Sakata, *Prog. Theor. Phys.* **28** (1962) 870.
- [31] E. K. Akhmedov, *Phys. Lett. B* **503**, 133 (2001) [arXiv:hep-ph/0011136].
- [32] A. S. Dighe and A. Y. Smirnov, *Phys. Rev. D* **62**, 033007 (2000) [arXiv:hep-ph/9907423].
- [33] S. T. Petcov, *Phys. Lett. B* **200**, 373 (1988).
- [34] J. G. Learned and S. Pakvasa, *Astropart. Phys.* **3**, 267 (1995).
- [35] E. Bugaev, T. Montaruli, Y. Shlepin and I. Sokalski, *Astropart. Phys.* **21**, 491 (2004); T. DeYoung, S. Razzaque and D. F. Cowen, *Astropart. Phys.* **27**, 238 (2007).